Experimental Analysis of Hydrodynamics in a Radially Agitated Tank

Renaud Escudié and Alain Liné
Laboratoire d'Ingénierie des Procédés de l'Environnement, Institut National des Sciences Appliquées de Toulouse, 31077 Toulouse Cedex, France

A PIV technique is used to analyze the local hydrodynamics generated by a Rushton turbine. Different types of motion coexist in the tank: the mean flow (or global circulation), the periodic fluctuations (or trailing vortices) induced by the blade rotation in the impeller region, and the turbulent fluctuations (that dissipate the kinetic energy). These three kinds of motion can be estimated after experiments as soon as a triple decomposition of the velocity is performed. The mean velocity, the periodically induced stress, and the Reynolds stress are analyzed in the agitated tank, close to the impeller. These data are used for two purposes: to identify and quantify the transfer of kinetic energy between mean flow, periodic flow, and turbulence; and to estimate the dissipation rate of turbulent kinetic energy (TKE) from the balance of TKE, in which each term will be derived from experiments. Characteristics of turbulence are also presented and discussed.

Introduction

Stirred-tanks equipped with a Rushton turbine are mainly used in industry, and a large amount of literature on this equipment has been published over many years. However, mixing mechanisms are not yet fully understood. The respective roles of global circulation, trailing vortices, and small-scale turbulence on macromixing and micromixing is not so clear. These different types of motion coexist in the tank: the mean flow (or global circulation), the periodic fluctuations (or trailing vortices) induced by the blade rotation in the impeller region, and the turbulent fluctuations (that finally dissipate the kinetic energy).

The following points will be introduced and briefly reviewed. The experimental technique used to analyze the flow field will be recalled. The main results obtained from global studies will be listed. More detailed studies of local hydrodynamics have been based on the decomposition of the velocity fluctuations between turbulent and organized motions. Different decomposition techniques will be recalled. The main results obtained after decomposition will be presented in terms of kinetic energy of turbulence and kinetic energy of organized motion. In addition, turbulence characteristics, including length scales and the dissipation rate of turbulent kinetic energy, will be reviewed. The specific study of trailing vortices is beyond the scope of this article.

Correspondence concerning this article should be addressed to A. Liné.

Experimental technique

Mavros (2001) reviewed the experimental techniques available for studying the flow patterns in stirred vessels: photographic technique (Cutter, 1966), hot-wire anemometry (Mujumbar et al., 1970), laser-Doppler velocimetry (Costes and Couderc, 1988; Mahouast et al., 1989; Wu and Patterson, 1989; Kresta, 1991; Stoots and Calabrese, 1995; Lee and Yianneskis, 1998), ultrasound Doppler velocimetry (Bouillard et al., 2001), and particule image velocimetry (PIV; Hill et al., 2000; Sheng et al., 2000; Escudié, 2001; Sharp and Adrian, 2001). Such techniques were used to perform velocity measurements in the case of the Rushton turbine. The present work is based on the PIV technique that enables the measurement of an instantaneous velocity field in a plane. The main limitation of the technique is related to the spatial filter induced by the image processing; this will be discussed in detail. The size of the filter will be compared to the Taylor microscale, in order to ensure that energetic fluctuations are not filtered.

Main results obtained after global studies

The objectives of global studies were to determine the global circulation in the tank. For example, the radial mean velocity (Table 1) was investigated in the jet of the impeller (Cutter, 1966; Mujumbar et al., 1970; Costes and Couderc,

Table 1. Maximal Radial Mean Velocity at the Impeller Tip

	Radial Component $\overline{U_1}/U_{tip}$
Van der Molen and Van Maanen (1978)	0.85
Yianneskis et al. (1987)	0.7
Wu and Patterson (1989)	0.78
Ranade and Joshi (1990)	0.7
Stoots and Calabrese (1995)	0.87
Lee and Yianneskis (1998)	0.74
Present work	0.80

1988). At the same position in the tank, the ratio of the mean velocity components, normalized by the velocity of the impeller tip ($U_{tip} = \pi ND$), was shown to be independent of the impeller diameter (D) (or the tank diameter $T = 3D$) and of the agitator rotational speed (N) (Cutter, 1966; Van der Molen and van Maanen, 1978; Costes and Couderc, 1988; Wu and Patterson, 1989).

Despite the use of a standard stirred-vessel configuration, the results obtained by different authors can show significant differences, as pointed out by Yianneskis (2000). The source of these inconsistencies can be attributed to a small difference in the stirred-vessel configuration. The presence of bolts, used to fix the blades to the hub, for example, can affect the mean flow and the trailing vortex structure. Moreover, the thickness of the disk or impeller blades can influence significantly the hydrodynamic characteristics (Rutherford et al., 1996). Keeping this observation in mind, our results will be compared to these previous works.

Decomposition techniques

In the past, several techniques were used to separate the velocity fluctuations due to the turbulence from the organized motion generated by the impeller-blade rotation (and related to trailing vortices). Signal processing enables the organized motion to be extracted from the total fluctuations in terms of temporal or spectral analysis:

- The velocity correlation function was shown to be composed of a periodic component added to a random one (Mujumbar et al., 1970; Wu and Patterson, 1989)
- The energy spectrum was shown to exhibit a classic shape, with additional peaks related to the impeller frequency (Cutter, 1966; Van der Molen and Van Maanen, 1978; Costes and Couderc, 1988; Mahouast et al., 1989).

These two techniques require high-frequency measurement (LDV, Hot-wire Anemometry), and cannot be applied in the case of the PIV technique.

Since the organized motion is generated by the blades, a synchronization of the data acquisition with the blade position can be used to separate periodic and turbulent fluctuations (Van der Molen and Van Maanen, 1978; Yianneskis et al., 1987; Yianneskis and Whitelaw, 1993; Stoots and Calabrese, 1995; Schaffer et al., 2000; Sharp and Adrian, 2001). Moreover, this technique enables the organized motion velocity to be extracted for a given blade position relative to the measurement plane: the trailing vortices can then be visualized. This technique will be used in the present study. In order to synchronize the acquisition, an encoder will be mounted on the impeller shaft.

Turbulent kinetic energy and periodic motion kinetic energy

The turbulent kinetic energy and the organized motion kinetic energy can be obtained after the decomposition technique presented earlier. Kinetic energy is usually normalized by U_{tip}^2 (Cutter, 1966; Wu and Patterson, 1989). In the impeller tip region, the kinetic energy of the organized motion is significant (Wu and Patterson, 1989; Mahouast et al., 1989). With increasing radial position, two main characteristics can be pointed out: the organized motion kinetic energy decreases and the turbulent kinetic energy first increases and then decreases. Van der Molen and Van Maanen (1978) suggested that a link seems to exist between turbulence and trailing vortices. Indeed, phase-averaged measurements show that the turbulent kinetic energy is higher in the trailing vortex region than elsewhere in the jet (Lee and Yianneskis, 1998; Schaffer et al., 1997; Ranade et al., 2001; Sharp and Adrian, 2001). However, the interaction is not yet clearly defined. One of the objectives of the present work is to quantify the energy transfer between trailing vortices and turbulence, in order to improve the understanding.

Turbulence characteristics: Anisotropy and scales

In the turbulent regime, the fluid dynamic is characterized by a wide range of length scales. Three kinds of scales can be identified: the Kolmogorov scale, η, the Taylor microscale, λ, and the macrolength scale Λ.

In the energy-cascade theory, the smallest turbulent structures are called Kolmogorov scale, denoted by η. At this scale, the turbulent kinetic energy is dissipated by molecular viscosity. The scale η can be expressed in terms of the dissipation rate of turbulent kinetic energy, ϵ, and kinematic viscosity ν, as follows

$$\eta = \left(\frac{\nu^3}{\epsilon}\right)^{1/4} \tag{1}$$

The Taylor microscale, λ, has a size characterized by the smallest energetic structures. In the case of isotropic turbulence, the Taylor microscale can be expressed in terms of dissipation rate of kinetic energy ϵ and turbulent kinetic energy k (Sharp and Adrian, 2001)

$$\lambda = \sqrt{\frac{15\nu\overline{u'^2}}{\epsilon}} = \sqrt{\frac{10\nu k}{\epsilon}} \tag{2}$$

The macrolength scale, Λ, corresponds locally to the size of the most energetic turbulent structure. The temporal macroscale (t_E) can be estimated using the single-point measurement technique. The Taylor hypothesis (frozen turbulence) can be used to calculate the spatial macroscale. One of the advantages of the PIV technique is to directly determine the macroscale, after spatial correlation of the turbulent velocity field measured in a plane (Bugay, 1998). The macroscale, Λ, was usually normalized with the impeller width, w (Costes and Couderc, 1989; Michelet, 1998). However, turbulence is anisotropic, and macroscales are different in the three directions of the Cartesian reference frame (Cutter, 1966; Wu and Patterson, 1989; Bugay, 1998).

Table 2. Macrolength Scales in the Stream Jet

	Λ/w
Cutter (1966)	$0.14 < \Lambda/w < 0.2$ (tangential direction) $0.25 < \Lambda/w < 0.45$ (radial direction)
Mujumbar et al. (1970)	$0.2 < \Lambda/w < 0.5$
Costes and Couderc (1988)	$\Lambda/w \approx 0.5$
Mahouast et al. (1989)	$0.48 < \Lambda/w < 1.32$
Wu and Patterson (1989)	$0.35 < \Lambda/w < 0.50$ (radial direction) $\Lambda/w \approx 0.5$ (tangential direction) $0.25 < \Lambda/w < 0.4$ (vertical direction)
Lee and Yianneskis (1998)	$0.1 < \Lambda/w < 0.3$
Michelet (1998)	$0.6 < \Lambda/w < 1.2$

The macroscales were shown to depend on radial and axial locations in the tank (Table 2). In the impeller jet, the smallest scales are located close to the impeller tip. With increasing radial position, the macroscale increases (Mahouast et al., 1989; Wu and Patterson, 1989; Michelet, 1998). Outside the impeller zone, the order of magnitude of the macroscale was shown to be D/4.4 (Costes and Couderc, 1988) or D/4 (Ranade and Joshi, 1990; Michelet, 1998). These different scales will be determined in the present work.

Dissipation rate of turbulent kinetic energy

The determination of the local dissipation rate of turbulent kinetic energy, ϵ, is important. However, the direct measurement of ϵ is very difficult, since it needs to capture precisely the smallest turbulent structures (Saarentine and Piirto, 2000).

In the past, several methods were developed to estimate the dissipation rate of turbulent kinetic energy:

- Kinetic energy balance term averaged over a control volume (Cutter, 1966; Wu and Patterson, 1989; Zhou and Kresta, 1996a)
- Integration of dissipation spectrum (Okamota et al., 1981; Costes and Couderc, 1988)
- Dimensional analysis (Zhou and Kresta, 1996b)

$$\epsilon = A\frac{u'^3}{L} \tag{3}$$

where A is a constant, u' is a turbulent velocity characteristic, and L is a length-scale characteristic. The length scale, L, can be taken as proportional to the impeller diameter, D: $L = D$ (Costes and Couderc, 1988), $L = D/2$ (Stoots and Calabrese, 1989), $L = D/10$ (Kresta and Wood, 1991). In some cases, L is the spatial macroscale (Λ) and is determined from experiments (Cutter, 1966; Wu and Patterson, 1989; Bugay, 1998). However, this dimensional analysis assumes that the turbulence is fully developed. Indeed, the time needed to obtain fully developed turbulence can be defined as follows

$$\frac{L}{\sqrt{k/3}} \tag{4}$$

In the stream jet of a Rushton turbine, Michelet (1998) estimated the distance covered during this time as $0.6D$ (where D is the impeller diameter). Considering that the impeller generates the turbulence, Eq. 3 cannot be used to estimate the dissipation rate of turbulent kinetic energy, ϵ.

- The dissipation rate of turbulent kinetic energy ϵ can be estimated from the balance equation of turbulent kinetic energy. In this case, most of the terms of the equation are calculated from experiments and the dissipation rate can be deduced. The dissipation rate, ϵ, was estimated in the case of a shaped impeller (Lightnin A310; Bugay et al., 2002).
- Michelet (1998) estimated ϵ directly using the two-point measurement LDV technique.
- Sharp and Adrian (2001) derived ϵ directly using the PIV technique.

Most of the authors agree on the fact that 20% to 30% of the energy transferred to the fluid by the impeller is dissipated in the region of the impeller. In the present work, the dissipation will be estimated from local balance of TKE.

Discussion

In the present study, the PIV technique is used to analyze the local hydrodynamics generated by a Rushton turbine. Recently, Sharp and Adrian (2001) published an article based on similar experiments using the PIV technique to analyze the small-scale flow structure around a Rushton turbine; in their article, they focused on the direct estimation of the TKE dissipation rate. In our case, the spatial resolution of the PIV measurement being larger, the TKE dissipation rate cannot be directly estimated. The data have to be processed differently. The estimation of the TKE dissipation rate is based on the balance equation of TKE, in which each term is derived from experiments. To achieve this balance, the different types of kinetic energy will be analyzed and the importance of the exchanges of kinetic energy between turbulence and trailing vortices will be emphasized.

The different types of kinetic energy are basically related to the different types of motion generated in the tank: the mean flow, the periodic fluctuations induced around the impeller by the blade rotation, and the turbulent fluctuations. The balances of these different types of kinetic energy will be analyzed and their transfer will be discussed. Indeed, the balance equations of different types of kinetic energy were derived by Reynolds and Hussain (1972). The authors performed a triple decomposition of the velocity in order to determine turbulence in the presence of periodic flow. It will be shown in the current article that many terms of these balance equations can be estimated from experiments. Such balance equations enable the terms that cannot be directly measured to be estimated, namely, diffusion terms involving pressure fluctuations or the dissipation rate of TKE.

Estimation of the terms involved in the balance equations supposes the use of reliable data. Therefore, in the first step of this study, the present data are validated after a comparison with previous experimental works. Once the data are validated, data processing can be developed in order to understand the exchange of energy between the different motions.

In the first part of this article, the principles of the PIV technique are recalled. Then, the experimental setup is presented. The mean velocity field and the Reynolds stress components are analyzed and validated in the case of the radially agitated tank. These data are then used to estimate the dissipation rate of TKE. The dissipation rate of TKE is deduced

from the balance of TKE after precisely estimating transport, dissipation, and transfer terms. The characteristic length scales of turbulence are then analyzed.

Experimental Study

PIV technique

The principle of the PIV technique consists in acquiring instantaneous two-dimensional (2-D) velocity fields. The PIV technique is based on the following steps:

- Seeding the fluid-flow volume under investigation with small solid particles;
- Illuminating a slice of the flow field with a pulsing light sheet in order to visualize particles location;
- Recording two images of the fluid flow with a short time interval between them, using a digital CCD camera;
- Processing these images by dividing the complete image into squared interrogation areas. In each 32-pixels wide interrogation area, the cross-correlation technique enables the most probable particle displacement to be calculated: given the time delay between two successive images, the instantaneous velocity can be calculated. This technique is applied to the complete image from the camera in order to get the instantaneous velocity field.

The PIV system used was the commercial system acquired from Dantec Measurement Technology. The system includes a laser (Mini Yag, 15 Hz, 30 mJ), a double-image recorder camera (Kodak Megaplus ES 1.0, 1008×1018 pixels), a dedicated processor (PIV 2000), and the software. The processor does all the calculations in real time. As the processor produces vector maps, they are displayed and optionally stored by the software. The software also automatically generates all the synchronization signals for system integration. The seeding material is spherical hollow glass silvered particles from Dantec (density = 1.4, 10 μm $< d_p <$ 30 μm).

Experimental apparatus

The apparatus used in this study consisted of a standard cylindrical tank equipped with a Rushton turbine (Figure 1). The cylindrical tank was made of glass (6 mm thick) and had a diameter $T = 450$ mm and a liquid height $H = T = 450$ mm. The cylindrical vessel was placed in a cubic tank filled with tap water to minimize optical refraction. Four equally spaced baffles made of glass (width $B = 45$ mm $= T/10$) were fitted along the internal surface of the vessel. The tank, filled with tap water as the working fluid, was open at the top. The Rushton turbine was of standard design with a diameter $D = T/3 = 150$ mm. The clearance, C, was equal to the impeller diameter and was measured between the bottom of the mixing vessel and the impeller-disk plane. The blade height, w, was 0.2 D. Both the blade thickness, t_b, and the disk thickness, t_d, are equal to 2 mm.

The orientation of the Cartesian reference frame is plotted in the Figure 1. X_1 corresponds to the radial direction (positive toward the tank wall), X_2 the tangential direction, and X_3 the vertical direction (positive toward the tank top).

Experiments were carried out at a single value of impeller rotational speed $N = 150$ rpm. The Reynolds number ($Re = (ND^2)/\nu$) is then equal to 56,250. The flow pattern is turbulent. The pumping number is defined as

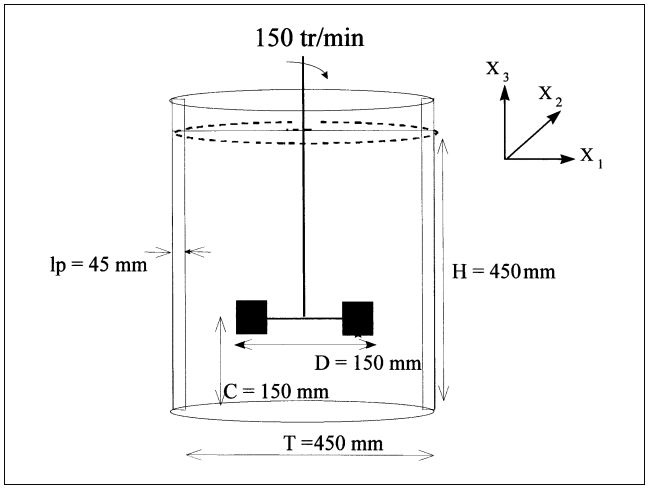

Figure 1. Tank geometry.

$$N_{Q_p} = \frac{Q_p}{ND^3} \tag{5}$$

and is equal to 0.68 (Roustan et al., 1999) and corresponds to a pumping flow rate of 5.7 L·s^{-1}. If the fluid is assumed to flow radially through the surface of a cylinder described by the impeller tip (with a diameter corresponding to the impeller diameter, D, and a height corresponding to the blade width, $w = 30$ mm), the surface area is then equal to and $S = \pi Dw = 0.014$ m^2 the mean velocity is 0.4 m·s^{-1}.

The power number is defined as

$$N_P = \frac{P}{\rho N^3 D^5} \tag{6}$$

and is equal to 5.5 (Roustan et al., 1999). It corresponds to power, $P = 5.9$ kg·m^2/s$^3 = 5.9$ W. The volume (ϑ) of liquid in the tank is 70 L. The power number corresponds to a volume average of the dissipation rate of kinetic energy equal to

$$\langle \epsilon \rangle_{\tan k} = \frac{P}{\rho \vartheta} = 0.11 \text{ m}^2/\text{s}^3 \tag{7}$$

Accuracy of data acquisition

The accuracy of the velocity measurements depends on different parameters such as the seeding concentration, the size of the PIV measurement area, the time interval between two laser slices, and the spatial resolution. Indeed, a compromise has to be found between two opposing goals:

- The size of the measurement area should be as large as possible in order to determine the velocity field in a large domain;
- The spatial resolution should be small enough so that any turbulent eddy that is too small to be measured has an insignificant energy value.

Consequently, two preliminary tests were performed to choose the best measurement area size:

- In the first experiment, data were obtained with a measurement area of 60×60 mm^2. Such a measurement domain

is relatively large compared to the experiments of Sharp and Adrian (2001), and relatively small compared to the full size of the tank. In fact, the measurement domain is restricted to a region of the jet close to the impeller tip. This is the domain where the exchange of kinetic energy between organized motion and turbulence are the most significant. Using the PIV technique, the domain is divided in an interrogation area. The size of the 32-pixels-by-32-pixels interrogation area is 2.2×2.2 mm^2. Interrogation areas are not adjacent, but 50% overlapped. Hence, a vector is measured every 1.1 mm.

- In the second experiment, data were obtained with a smaller measurement area of 30×30 mm^2. Given similar experimental conditions, the size of the interrogation area is 1.1×1.1 mm^2, and a vector is measured every 0.55 mm.

The results obtained after these two experiments, performed in only one plane, are compared in terms of profiles of the two components of the mean velocity vector and in terms of the three components of the stress tensor. The vertical profiles of both radial and axial components of the mean velocity normalized with U_{tip} are plotted at two radial positions ($r/R = 1.15$ and $r/R = 1.45$) in Figures 2a and 2b, respectively. The mean velocity profiles obtained with the two experiments are shown to be similar; thus, the accuracy of the measurement of the mean velocity does not depend on the size of these interrogation areas. The vertical profiles of the sum of the two diagonal components of the Reynolds stresses normalized with U_{tip}^2 are plotted at the same radial positions in Figure 2c, and the profiles of the nondiagonal component of the Reynolds stress are plotted in Figure 2d. Once again, the profiles of Reynolds stresses do not depend on the size of the interrogation area. This proves that the larger measurement area does not significantly affect the total energy measured. Consequently, in the subsequent experiments, the larger measurement area will be used to determine both the mean flow and turbulence characteristics.

Indeed, this result can be argued by evaluating the Taylor microscale (Eq. 2). According to the experiments, the turbulent kinetic energy, k, ranges between 0.1 and 0.15 m$^2 \cdot$s^{-2} and its dissipation rate, ϵ, ranges between 1.5 and 5 m$^2 \cdot$s^{-3} in the region close to the impeller. The order of magnitude of the Taylor microscale, λ, then ranges between 0.45 and 1 mm. This order of magnitude corresponds to the spatial resolution of the current experiments.

The seeding concentration was adjusted in order to have between 5 and 10 particles in the interrogation region. The time delay between laser flashes depends on local hydrodynamics. For example, the size of the interrogation area is fixed at 2.2 mm; the maximum radial velocity of the fluid in the impeller jet being close to 2 m/s, a 0.2-ms time delay between laser flashes was chosen in this region, since it corresponds to a particle displacement equal to 20% of the interrogation area size (Keane and Adrian, 1992).

Accuracy of data processing

The statistical-average calculation was performed on a series of 1,000 instantaneous velocity fields. Statistical convergence was checked on mean velocity, Reynolds stress components and third-order moments of fluctuating velocity The third-order moments of fluctuating velocity will be used to estimate the diffusion terms. The evolutions of the cumula-

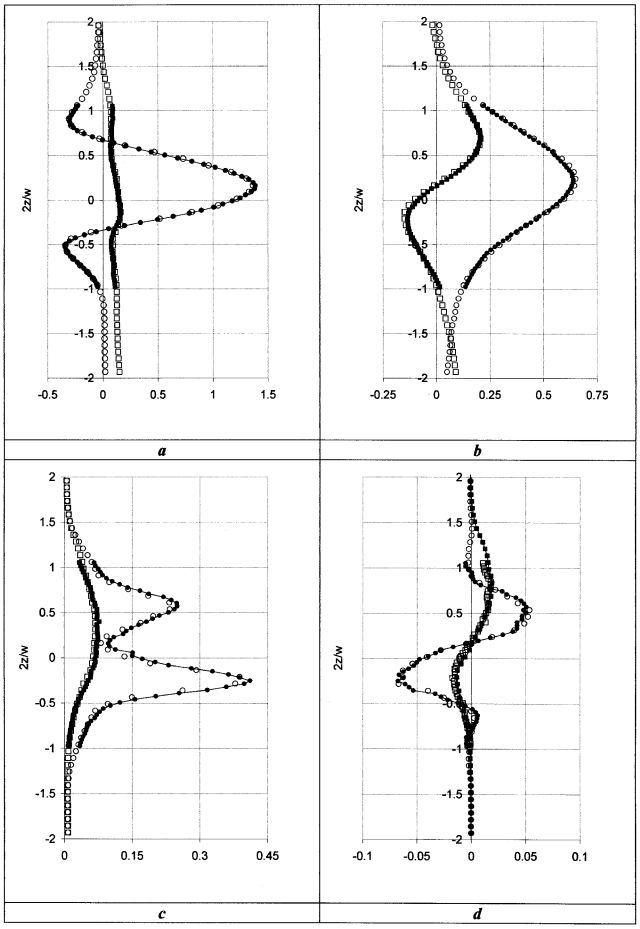

Figure 2. Vertical profile of mean velocity and turbulent components for the two interrogation sizes.

(a) Mean velocity at $r/R = 1.07$: −●− $\langle U_1 \rangle / U_{\text{tip}}$ (small size), ○ $\langle U_1 \rangle / U_{\text{tip}}$ (large size), −■− $\langle U_3 \rangle / U_{\text{tip}}$ (small size), □ $\langle U_1 \rangle / U_{\text{tip}}$ (large size); (b) mean velocity at $r/R = 1.45$; (c) diagonal component $((\langle u_1'^2 \rangle + \langle u_3'^2 \rangle)/U_{\text{tip}}^2)$ of Reynolds tensor: −●− $r/R = 1.15$ (small size), ○ $r/R = 1.15$ (large size), −■− $r/R = 1.45$ (small size), □ $r/R = 1.45$ (large size); (d) nondiagonal component $(\langle u_1' u_3' \rangle / U_{\text{tip}}^2)$ of Reynolds tensor: −●− $r/R = 1.15$ (small size), ○ $r/R = 1.15$ (large size), −■− $r/R = 1.45$ (small size), □ $r/R = 1.45$ (large size)

tive average of the mean velocity, the second and the third moment of fluctuating velocity, are plotted in Figures 3a−3c. The curves correspond to two velocity components measured at the fixed point $r/R = 1.33$, $2z/w = 1$, angular position = 20°.

Some vector measurements were considered to be spurious by the processor. They correspond to displacement vectors in the correlation plane, with peak heights that are rejected. Indeed, the processor locates the highest and second highest peak in the correlation plane. These two peaks are compared; the highest peak must be 1.2 times larger than the second one. If this is not the case, it means that there is too much noise, and the vector is then rejected. In the statistical-averaging procedure, these spurious vectors are ignored and the statistical average is determined on a reduced number of data, which takes the missing data into account. In our experiments, raw data were used as instantaneous velocity fields, without filtering and without move-averaging validation.

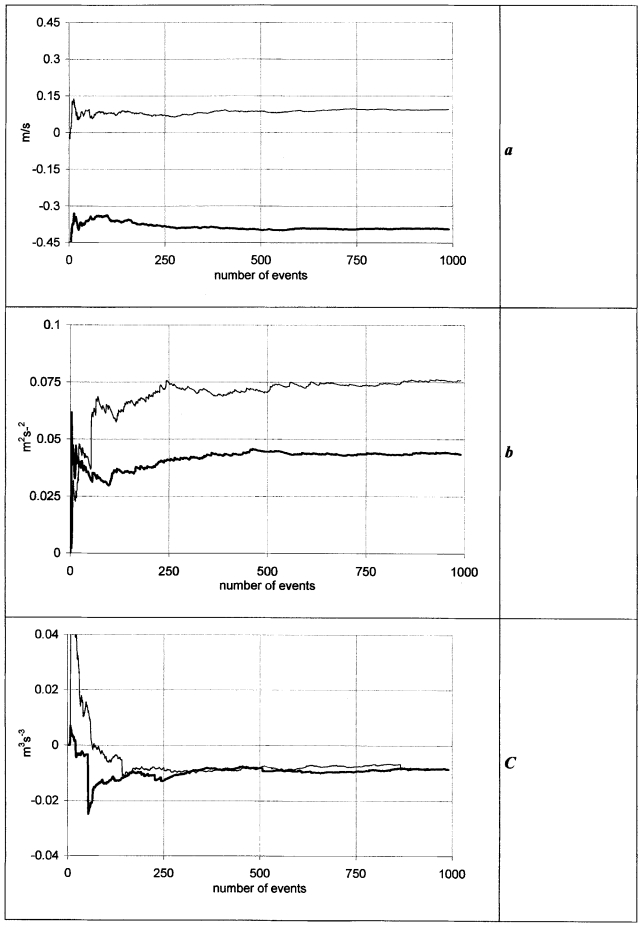

Figure 3. Statistical convergence.

(a) Mean velocity: — $\langle U_1 \rangle$, — $\langle U_3 \rangle$; (b) second moment: —— $\langle u_1'^2 \rangle$, — $\langle u_3'^2 \rangle$, (c) third moment: — $\langle u_1'^3 \rangle$, — $\langle u_3'^3 \rangle$.

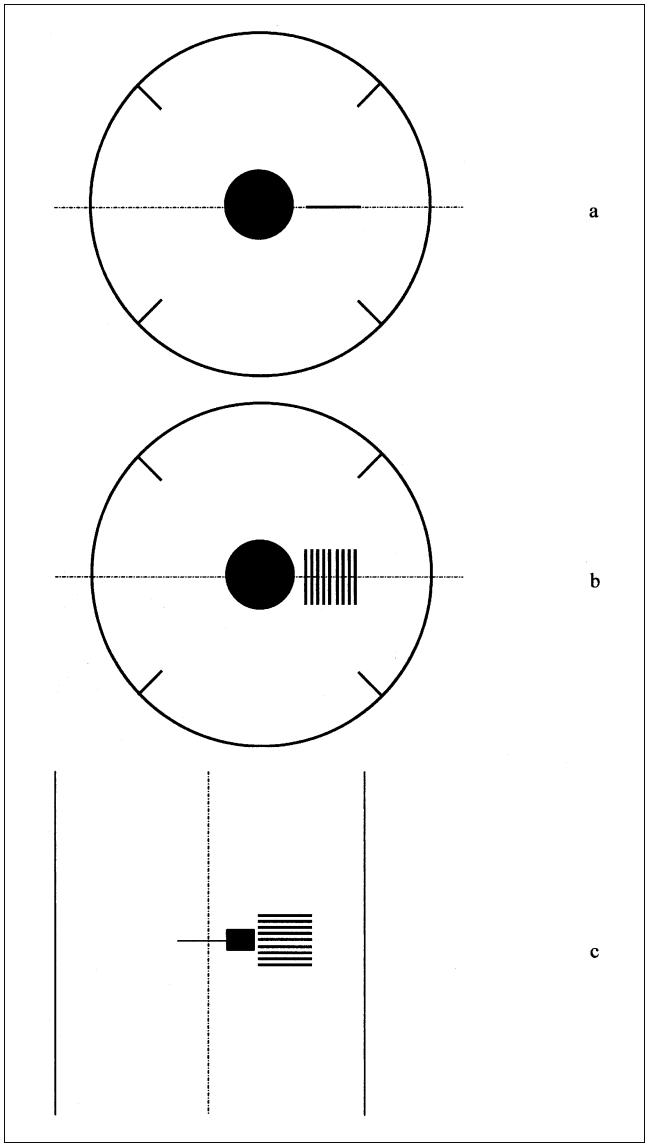

Figure 4. Measurement planes.

(a) Vertical plane ($X_1 - X_3$); (b) transversal planes ($X_2 - X_3$); (c) horizontal planes ($X_1 - X_2$).

The reproducibility of the measurements has been confirmed, since measurements were performed in three perpendicular planes in order to determine the three components of the velocity and the six components of the stress tensors: a first plane was necessary to measure U_1, U_2, a second plane was necessary to measure U_1, U_3, and a third plane was necessary to measure U_2, U_3. Hence, the data on instantaneous velocity components were systematically performed with two different planes and their values were compared to validate the measurements.

Measurement planes

The measurement plane is located in the region of the jet induced by the Rushton turbine, in a vertical plane of symmetry of the tank. The vertical plane is a bisector plane relative to two baffles.

In this study, the three components of the velocity vector and the six components of the stress tensor were measured. Moreover, it is necessary to calculate the gradient of these components in the three directions in the space. As a consequence, three kinds of the PIV measurement planes were performed:

(1) A vertical "radial" plane (Figure 4a) in order to calculate the components and their gradient in the $X_1 - X_3$ plane.

(2) Nine vertical "tangential" planes (Figure 4b) in order to calculate the components and their gradient in the $X_1 - X_2$ plane. Two successive planes are 5 mm apart.

(3) Nine horizontal planes (Figure 4c) in order to calculate the components and their gradient in the $X_2 - X_3$ plane. Two successive planes are also 5 mm apart.

Consequently, experimental data are available in a vertical plane, with the radial location ranging between r/R of 1.06 and 1.6, and with normalized axial direction ranging between $2z/w$ of -1.3 and 1.3. The impeller blade tip is situated at the radius $r/R = 1$, for axial position $2z/w$ ranging between -1 and 1.

Phase-average treatment

Angle-resolved measurements are made in each plane in order to determine the three components of the velocity vec-

tor and the six components of the Reynolds stress tensor. The region corresponding to the jet flow induced by the impeller is analyzed in detail. This choice is related to the analysis of different types of fluctuations induced by the impeller.

In the experiments, data acquisitions must be synchronized with the position of the impeller blades in order to perform the triple decomposition. The Rushton turbine is a six-blade impeller, the blades being equally spaced. As a consequence, given 1° angle-resolved measurements, it is necessary to perform 60 planes to reconstruct the flow between two successive blades. An encoder, mounted on the impeller shaft, enables the velocity-field measurement to be synchronized with one of the six blades of the impeller. PIV provides instantaneous velocity fields in one plane. In turbulent flow, it is necessary to decompose the instantaneous information $U_i^{lk}(M,t)$ in each k plane into the averaged velocity of the k plane $\langle U_i^k(M,t)\rangle$ and the turbulent fluctuation $u_i'^k(M,t)$ of the k plane

$$U_i^{lk}(M,t) = \langle U_i^k(M,t)\rangle + u_i'^{lk}(M,t) \tag{8}$$

As a consequence, the statistical average over a large number of events ($n_e = 1{,}000$) enables the calculation in each k plane of

- The average velocity of the k plane

$$\langle U_i^k(M,t)\rangle = \sum_{l=1}^{n_e} \frac{U_i^{lk}(M,t)}{n_e} \tag{9}$$

- The turbulent velocity correlation of the k plane

$$\langle u_i'^k(M,t)u_j'^k(M,t)\rangle = \sum_{l=1}^{n_e} \frac{u_i'^{lk}(M,t)u_j'^{lk}(M,t)}{n_e} \tag{10}$$

Considering the results of all the planes ($n_p = 60$), the average velocity of the flow and periodic fluctuation of each k plane can be calculated thanks to the decomposition

$$\langle U_i^k(M,t)\rangle = \overline{U_i}(M,t) + \tilde{u}_i^k(M,t) \tag{11}$$

Thanks to the statistical average over n_p planes, it is possible to determine the three major characteristics of the flow

- The mean velocity of the flow

$$\overline{U_i}(M,t) = \sum_{k=1}^{n_p} \frac{\langle U_i^k(M,t)\rangle}{n_p} \tag{12}$$

- The periodic tensor components

$$\overline{\tilde{u}_i(M,t)\tilde{u}_j(M,t)} = \sum_{k=1}^{n_p} \frac{\tilde{u}_i^k(M,t)\tilde{u}_j^k(M,t)}{n_p} \tag{13}$$

- The turbulent tensor components

$$\overline{u_i'(M,t)u_j'(M,t)} = \sum_{k=1}^{n_p} \frac{\langle u_i'^k(M,t)u_j'^k(M,t)\rangle}{n_p} \tag{14}$$

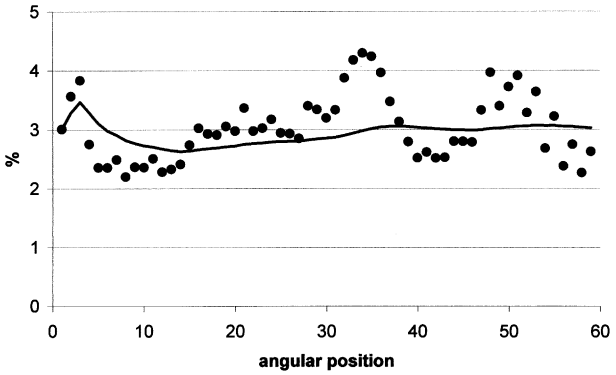

Figure 5. Divergence of the organized flow field.

● Value of $\nabla\cdot\tilde{u}^k/\max(|\partial\tilde{u}_i^k/\partial x_i|)$ averaged in the k plane; — cumulative error of $\nabla\cdot\tilde{u}^k/\max(|\partial\tilde{u}_i^k/\partial x_i|)$.

All of these different variables were determined experimentally. In the first step in this study, the profiles of the mean velocity, periodically induced, and the turbulence characteristics will be presented and discussed. In particular, the radial profile of TKE increases radially and then decreases. In order to understand this behavior, the balance of the different types of kinetic energy (mean, periodic and turbulent ones) will be analyzed in detail in the second step of this study. The exchanges of kinetic energy between the mean flow, the periodic motion, and the turbulence will be determined.

The reliability of the data resulting from the triple decomposition can be assessed. The phase-average flow field is almost divergence free. Indeed, $\nabla\cdot\tilde{u}^k$ has been evaluated from experiments in each vertical k plane ($k = 1, n_p$). The value of $\nabla\cdot\tilde{u}^k/\max(|\partial\tilde{u}_i^k/\partial x_i|)$ averaged in the k plane is plotted in Figure 5, and the cumulative error is also presented. The error is shown to be less than 3%.

Classical Results of Hydrodynamics Induced by a Rushton Turbine

Mean flow

The averaged velocity field induced by the turbine in the vertical plane is displayed in Figure 6. The radial jet generated by the impeller is not symmetrical, but is directed slightly upward. This result is in agreement with previous works (Wu and Patterson, 1989; Costes and Couderc, 1988; Derksen et al., 1998): it is not surprising, since first, the impeller is not symmetrically located ($C = T/3$), and second, the top of the tank is a free surface, whereas the bottom is a wall.

The profiles of the mean radial, tangential, and axial velocities normalized with the impeller tip velocity (U_{tip}) are plotted in the Figures 7a–7c at the impeller discharge boundary ($r/R = 1.07$). All velocity components are compared with results of earlier works (Zhou and Kresta, 1996a; Wu and Patterson, 1989; Rutherford et al., 1996). In Figure 7a, the two profiles relative to Rutherford et al. correspond to different blade thicknesses t_b (Rutherford et al. (1): $t_b/D = 0.0082$; Rutherford et al. (2): $t_b/D = 0.0204$). In the present tank configuration t_b/D equals 0.0133.

The flow pattern generated near the impeller tip is obviously a radial–tangential one. The radial velocity, $\overline{U_1}$, and

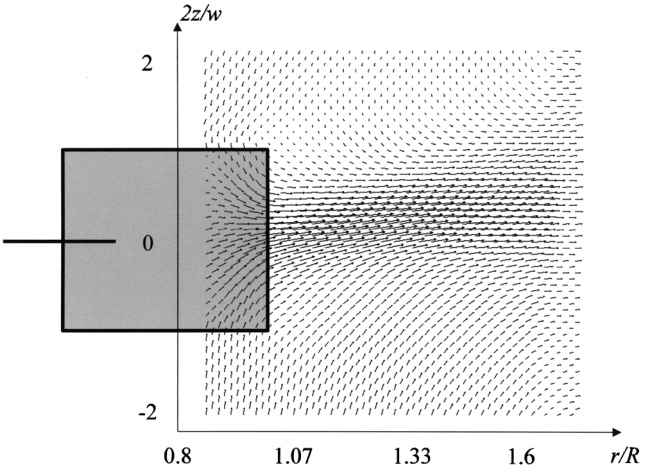

Figure 6. Mean velocity field in a vertical plane near impeller tip.

tangential one, $\overline{U_2}$, are maximal at the impeller tip and equal to 80% and 73% of the tip velocity, U_{tip}, respectively. In the jet, with increasing radial distance, the tangential velocity $\overline{U_2}$ decreases more rapidly than the radial component $\overline{U_1}$. The $\overline{U_1}/\overline{U_2}$ ratio equals 1.1 close to the tip, at the radial position $r/R = 1.07$; it increases along the stream jet ($\overline{U_1}/\overline{U_2} = 1.67$ at $r/R = 1.6$) because of the baffle effect. The axial velocity component $\overline{U_3}$ corresponds to the upward direction of the mean flow; its magnitude is much smaller than the other two.

The comparison of the different vertical profiles to previous data validates the present measurements. However, the difficulty in comparing different data sets was mentioned by Yanneskis (2000): the fact of plotting the mean velocity and vertical position relative to the impeller tip speed (U_{tip}) and to the impeller height (w) is sufficient for comparing data only if the stirred-tank geometries are exactly the same. In practice, this is rarely the case, and a slight difference in blade or disk thickness can affect both the mean flow and turbulence distributions (Rutherford et al., 1996; Yianneskis, 2000). Geometrical differences could explain the profile discrepancies: the clearance and the impeller diameter for the data of Zhou and Kresta (1996a) ($C = D = T/2$), and the blade thickness for the data of Rutherford et al. (1996). For the radial and axial velocity components, agreement with Wu and Patterson's data is especially good; a slight difference in baffle characteristics may explain the difference observed for the tangential component [unfortunately, no information on baffle geometry is reported in Wu and Patterson's (1989) article].

Turbulence and periodic flow

Contours of turbulent kinetic energy, k, periodic kinetic energy, $\tilde{k}$, and total fluctuating kinetic energy, k_{total}, normalized with U_{tip}^2, are plotted in Figures 8a, 8b and 8c, respectively, in the vertical plane of the measurement. If a simple Reynolds decomposition is performed in the tank (without phase averaging), the total fluctuating kinetic energy is measured: this energy cannot be physically analyzed close to the impeller blades, because random turbulent fluctuation and periodic fluctuation induced by the blade are not distinguishable:

$$k_{\text{total}} = k + \tilde{k} \tag{15}$$

The total kinetic energy (Figure 8c) is high in the jet, in the vicinity of the impeller. Up to a radial position of r/R equal to 1.5, a homogeneous distribution occurs with values ranging between 0.12 and 0.28. The value drops rapidly after this point. The periodic kinetic energy is concentrated in the vicinity of the impeller tip: the maximum level is 0.13 at $r/R = 1.07$, and only 0.02 at $r/R = 1.6$. Indeed, in the region near the impeller blade, the tangential velocities of the trailing vortices are higher and the associated periodic energy is significant. The trailing vortices vanish far from the impeller region. The radial variation in the turbulent kinetic energy is more surprising. The intensity increases by a factor of 2 between the impeller tip and radial position $r/R = 1.4$; further away, the turbulent kinetic energy decays rapidly. The increase in turbulent kinetic energy is significant and could be related to the decrease in periodic kinetic energy in the same region, the total fluctuating kinetic energy remaining relatively constant. As a consequence, the kinetic energy exchange may exist between periodic and turbulent components. A goal of this study was to identify and characterize the kinetic energy exchange between mean, periodic, and turbulent motions.

Vertical profiles of both turbulent and periodic kinetic energy components near the impeller tip are plotted in Figure 9. In order to validate the measurements, the results are compared to data from previous works. A very good agreement is found with Wu and Patterson's (1989) experiments.

In the center of the tank, more than 80% of the total kinetic energy is periodic. It is, thus, essential to perform phase averaging. In conclusion, the PIV technique and triple decomposition enable the 3-D mean flow induced by the Rushton turbine to be measured, along with all the components of both the Reynolds tensor and periodic stress tensor. The present data have been validated and are available to calculate most of the terms of the kinetic energy balance of the mean, turbulent, and periodic flow.

Triple Decomposition Technique and Results

Near the impeller, the velocities show different kinds of fluctuation: some fluctuations are purely turbulent, while others are induced by the periodic motion of the impeller blades. These latter fluctuations do not behave like turbulence and must be accounted for in a different way. In order to account for periodic blade motion, a triple decomposition must be performed

$$U_i = \overline{U_i} + \tilde{u}_i + u'_i \tag{16}$$

where U_i is the instantaneous velocity, $\overline{U_i}$ is the averaged velocity, $\tilde{u}_i$ is the periodic fluctuation, and u'_i is the turbulent fluctuation.

Reynolds and Hussain (1972) used this triple decomposition to establish the dynamical equations for the three motions. Starting with the Navier–Stokes equations, they obtained the continuity and momentum equations for the mean

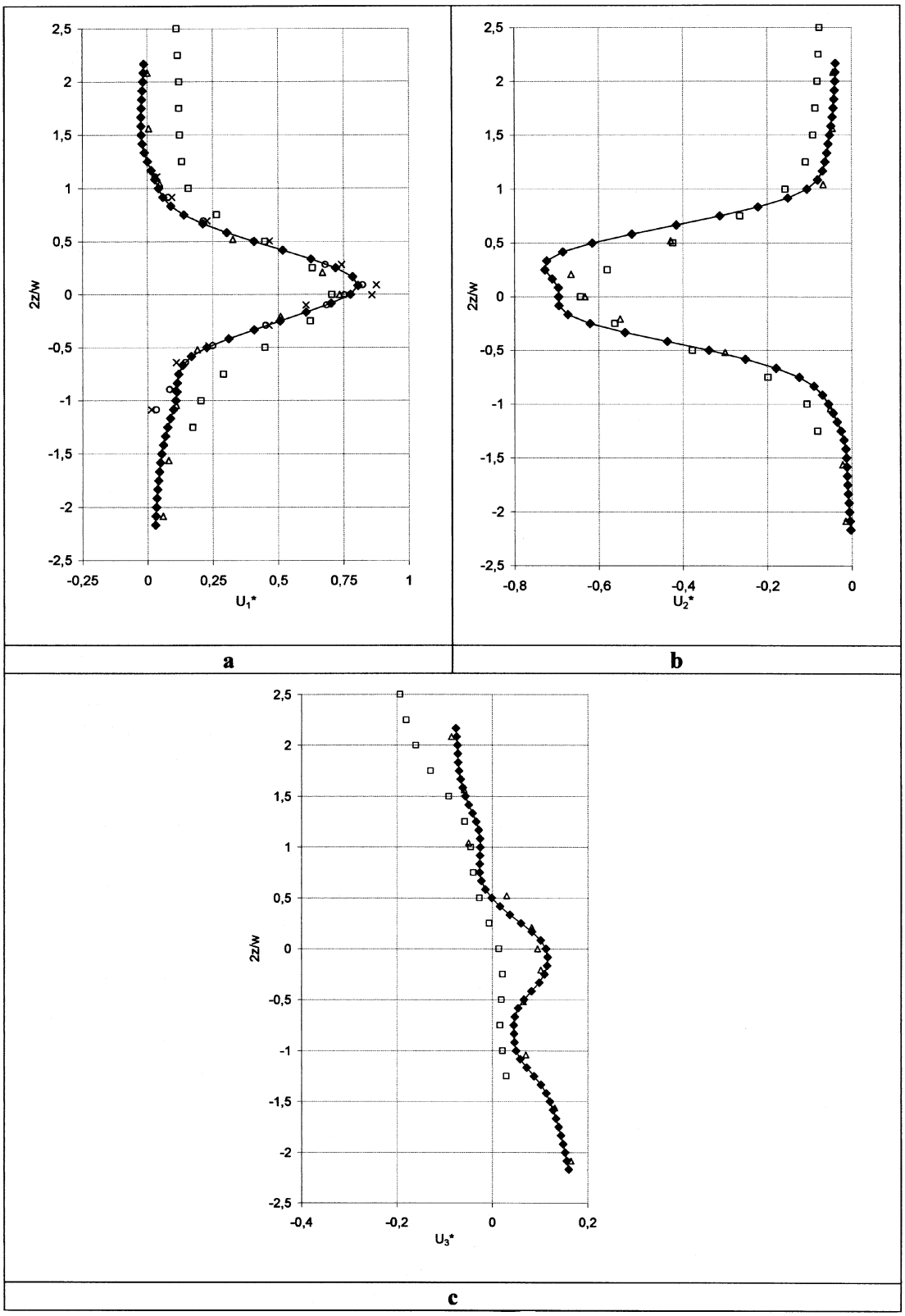

Figure 7. Vertical profiles of normalized mean velocity at $r/R = 1.07$.

– ♦ – Present work; □ Zhou and Kresta (1996); △ Wu and Patterson (1989); × Rutherford et al. (1996) $t_b/D = 0.0082$; ● Rutherford et al. (1996) $t_b/D = 0.0204$. (a) Radial velocity $\overline{U_1}/U_{tip}$; (b) tangential velocity $\overline{U_2}/U_{tip}$; (c) vertical velocity $\overline{U_3}/U_{tip}$.

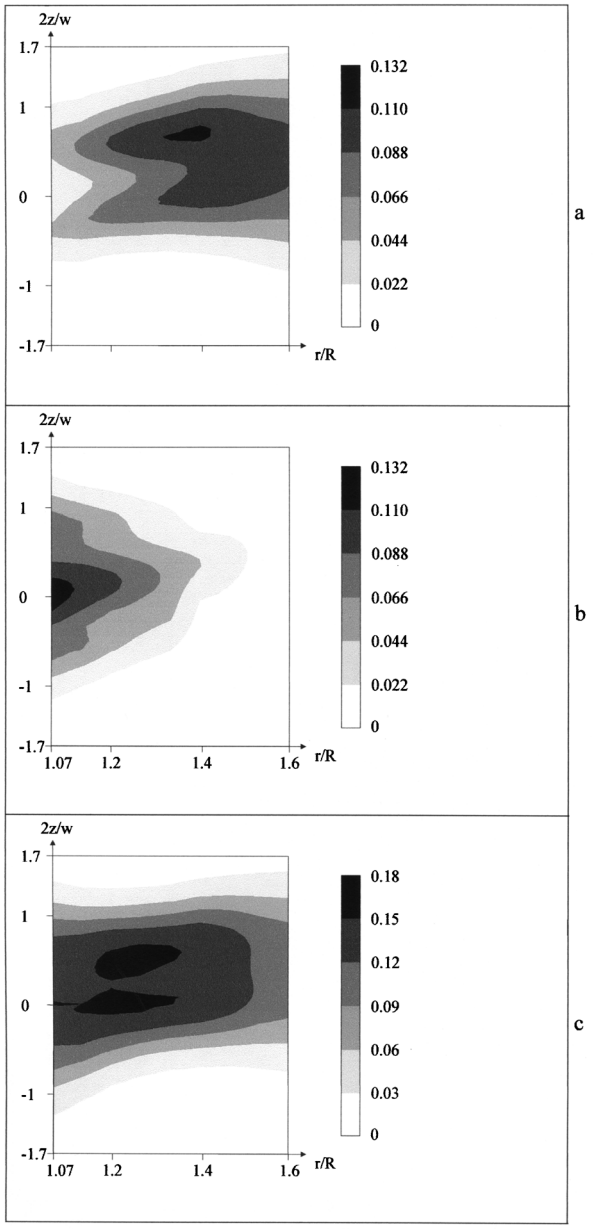

Figure 8. Contour of normalized kinetic energy in a vertical plane near impeller tip.

(a) Turbulent kinetic energy k/U_{tip}^2; (b) periodic kinetic energy $\tilde{k}/U_{tip}^2$; (c) fluctuating kinetic energy k_{total}/U_{tip}^2.

flow field

$$\frac{\partial \overline{U_i}}{\partial x_i} = 0 \tag{17}$$

$$\frac{\partial \overline{U_i}}{\partial t} + \underline{u_j}\frac{\partial \overline{U_i}}{\partial x_j} = -\frac{1}{\rho}\frac{\partial \bar{p}}{\partial x_i} + \nu\frac{\partial^2 \overline{U_i}}{\partial x_j^2} - \frac{\partial \overline{u_i' u_j'}}{\partial x_j} - \frac{\partial \overline{\tilde{u}_i \tilde{u}_j}}{\partial x_j} \tag{18}$$

In comparison with the classic Reynolds equation, an additional term $(\partial \overline{\tilde{u}_i \tilde{u}_j})/\partial x_j$ appears in Eq. 18. It involves the stresses $\overline{\tilde{u}_i \tilde{u}_j}$ induced by the organized motion generated by the blades.

Reynolds and Hussain (1972) obtained a kinetic energy balance between the three components of the total kinetic energy, as follows:

- Kinetic energy of mean flow

$$\underbrace{\frac{\partial}{\partial t}\left(\frac{1}{2}\overline{U_i}\,\overline{U_i}\right)}_{(1)} + \underbrace{\overline{U_j}\frac{\partial}{\partial x_j}\left(\frac{1}{2}\overline{U_i}\,\overline{U_i}\right)}_{(2)} = \underbrace{-\frac{1}{\rho}\frac{\partial \overline{P}\,\overline{U_i}}{\partial x_i}}_{(3)} \underbrace{-\left(-\overline{u_i' u_j'} - \overline{\tilde{u}_i \tilde{u}_j}\right)}_{(4)}$$

$$\underbrace{\frac{\partial \overline{U_i}}{\partial x_j} - \frac{\partial}{\partial x_j}\left[\overline{U_i}\left(-\overline{u_i' u_j'} - \overline{\tilde{u}_i \tilde{u}_j}\right)\right]}_{(5)} + \underbrace{\nu\frac{\partial}{\partial x_j}\left[\overline{U_i}\left(\frac{\partial \overline{U_i}}{\partial x_j} + \frac{\partial \overline{U_j}}{\partial x_i}\right)\right]}_{(6)}$$

$$\underbrace{-\frac{\nu}{2}\left(\frac{\partial \overline{U_i}}{\partial x_j} + \frac{\partial \overline{U_j}}{\partial x_i}\right)\left(\frac{\partial \overline{U_i}}{\partial x_j} + \frac{\partial \overline{U_j}}{\partial x_i}\right)}_{(7)} \tag{19}$$

where (1) is accumulation, (2) transport, (3), (5), and (6) diffusion, (4) transfer, and (7) dissipation.

- Kinetic energy of organized flow

$$\underbrace{\frac{\partial}{\partial t}\left(\frac{1}{2}\overline{\tilde{u}_i \tilde{u}_i}\right)}_{(1)} + \underbrace{\overline{U_j}\frac{\partial}{\partial x_j}\left(\frac{1}{2}\overline{\tilde{u}_i^2}\right)}_{(2)} = \underbrace{-\frac{1}{\rho}\frac{\partial}{\partial x_j}\left[\tilde{u}_j\left(\tilde{p} + \frac{1}{2}\rho\overline{\tilde{u}_i \tilde{u}_i}\right)\right]}_{(3)}$$

$$\underbrace{+\left(-\overline{\tilde{u}_i \tilde{u}_j}\right)\frac{\partial \overline{U_i}}{\partial x_j}}_{(4)} \underbrace{-\overline{\left(-\langle u_i' u_j'\rangle \frac{\partial \tilde{u}_i}{\partial x_j}\right)}}_{(5)} + \underbrace{\nu\frac{\partial}{\partial x_j}\left[\overline{\tilde{u}_i\left(\frac{\partial \tilde{u}_i}{\partial x_j} + \frac{\partial \tilde{u}_j}{\partial x_i}\right)}\right]}_{(6)}$$

$$\underbrace{-\frac{\nu}{2}\left(\frac{\partial \tilde{u}_i}{\partial x_j} + \frac{\partial \tilde{u}_j}{\partial x_i}\right)\left(\frac{\partial \tilde{u}_i}{\partial x_j} + \frac{\partial \tilde{u}_j}{\partial x_i}\right)}_{(7)} \tag{20}$$

where (1) is accumulation, (2) transport, (3) and (6) diffusion, (4) and (5) transfer, (7) dissipation.

- Kinetic energy of turbulence

$$\underbrace{\frac{\partial}{\partial t}\left(\frac{1}{2}\overline{u_i' u_i'}\right)}_{(1)} + \underbrace{\overline{U_j}\frac{\partial}{\partial x_j}\left(\frac{1}{2}\overline{u_i' u_i'}\right)}_{(2)} = \underbrace{-\frac{1}{\rho}\frac{\partial}{\partial x_j}\left[\overline{u_j'\left(p' + \frac{1}{2}\rho u_i' u_i'\right)}\right]}_{(3)}$$

$$\underbrace{+\left(-\overline{u_i' u_j'}\right)\frac{\partial \overline{U_i}}{\partial x_j}}_{(4)} \underbrace{+\left(-\langle u_i' u_j'\rangle \frac{\partial \tilde{u}_i}{\partial x_j}\right)}_{(5)} + \underbrace{\overline{\tilde{u}_j \frac{\partial}{\partial x_j}\left\langle \frac{1}{2}u_i' u_j'\right\rangle}}_{(6)}$$

$$\underbrace{+\nu\frac{\partial}{\partial x_j}\left(\overline{\tilde{u}_i\left(\frac{\partial u_i'}{\partial x_j} + \frac{\partial u_j'}{\partial x_i}\right)}\right)}_{(7)} \underbrace{-\frac{\nu}{2}\overline{\left(\frac{\partial u_i'}{\partial x_j} + \frac{\partial u_j'}{\partial x_i}\right)\left(\frac{\partial u_i'}{\partial x_j} + \frac{\partial u_j'}{\partial x_i}\right)}}_{(8)} \tag{21}$$

where (1) is accumulation, (2) transport, (3), (6) and (7) diffusion, (4) and (5) transfer, and (8) dissipation.

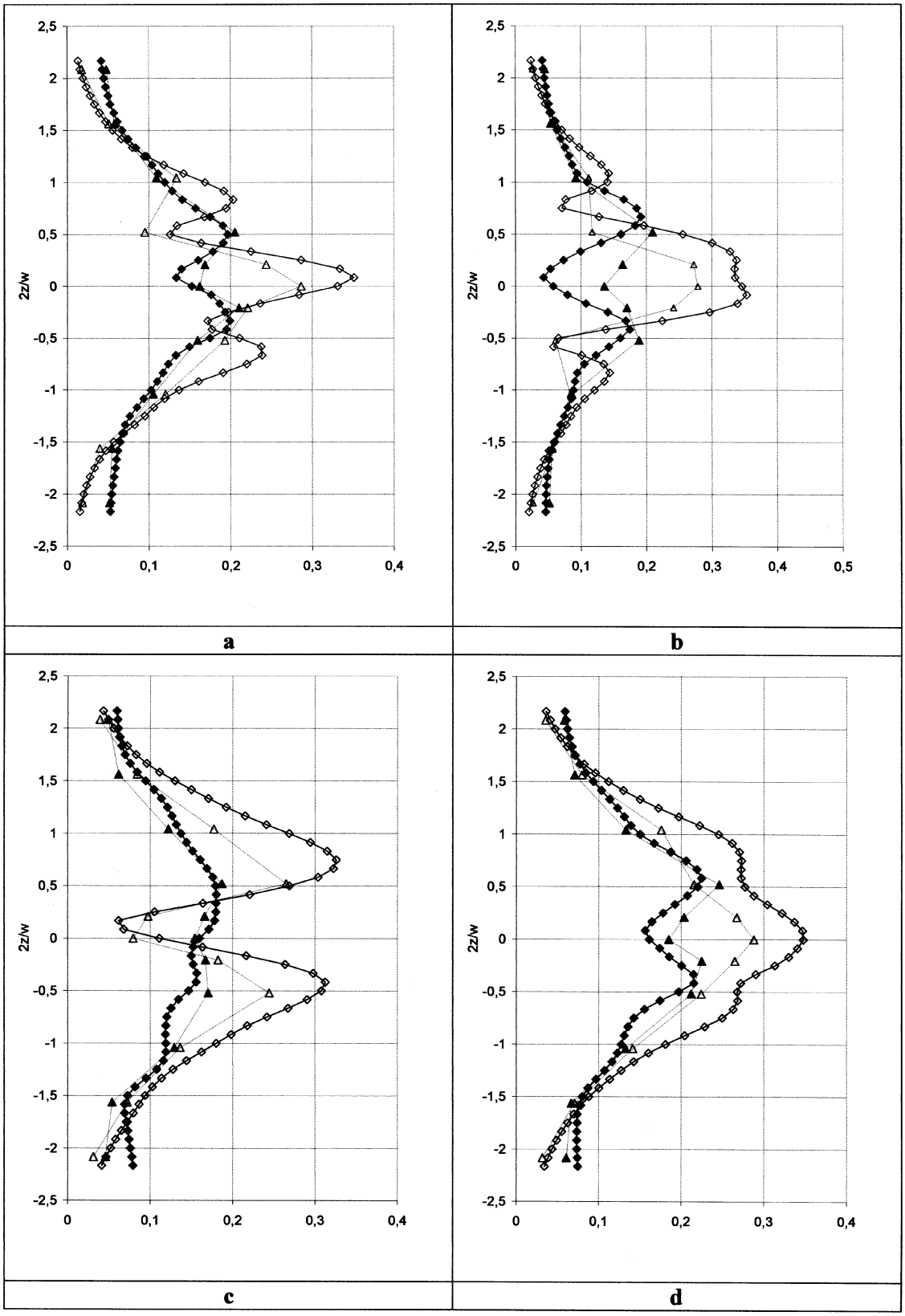

Figure 9. Vertical profile of normalized turbulent and periodic kinetic energy components at $r/R = 1.07$.

Turbulent kinetic energy: −♦− present work, --▲-- Wu and Patterson (1989); periodic kinetic energy: −◇− present work, --△-- Wu and Patterson (1989). (a) Axial component: $\overline{u_1'^2}/U_{tip}^2$ and $\overline{\tilde{u}_1^2}/U_{tip}^2$; (b) tangential component: $\overline{u_2'^2}/U_{tip}^2$ and $\overline{\tilde{u}_2^2}/U_{tip}^2$; (c) axial component: $\overline{u_3'^2}/U_{tip}^2$ and $\overline{\tilde{u}_3^2}/U_{tip}^2$; (d) kinetics energy components: k^2/U_{tip}^2 and $\tilde{k}/U_{tip}^2$.

The terms appearing in the equations represent transport, diffusion, viscous dissipation rate, and transfer of kinetic energy between the three motions. Indeed, three terms of exchange of kinetic energy appear as an energy "sink" or an energy "source"

• Kinetic energy transfer between mean and turbulent motion (*Tmt*):

$$Tmt = \sum_i \sum_j Tmt_{ij} = -\overline{u_i' u_j'} \frac{\partial \overline{U_i}}{\partial x_j} \tag{22}$$

• Kinetic energy transfer between mean and organized motion (*Tmo*)

$$Tmo = \sum_i \sum_j Tmo_{ij} = -\overline{\tilde{u}_i \tilde{u}_j} \frac{\partial \overline{U_i}}{\partial x_j} \tag{23}$$

• Kinetic energy transfer between organized and turbulent motion ($\overline{Tot}$)

$$\overline{Tot} = \overline{\sum_i \sum_j Tot_{ij}} = \overline{\left(-\langle u_i' u_j' \rangle \frac{\partial \tilde{u}_i}{\partial x_j} \right)} = \overline{\left(-r_{ij} \frac{\partial \tilde{u}_i}{\partial x_j} \right)}, \tag{24}$$

where

$$r_{ij} = \langle u_i' u_j' \rangle - \overline{u_i' u_j'} \tag{25}$$

The estimation of these three terms involves the measurement of the six components of the tensors of turbulent stresses ($\overline{u_i' u_j'}$) and organized stresses ($\overline{\tilde{u}_i \tilde{u}_j}$).

PIV investigations enable a majority of the terms that appear in the kinetic energy balance equations to be calculated. In the case of the balance of mean and organized flow, the diffusion terms due to pressure stresses [respectively $(1/\rho)(\partial \overline{P} \overline{U_i}/\partial x_i)$ and $(1/\rho)(\partial/\partial x_j)(\tilde{u}_j \tilde{p})$] can be estimated by a balance equation. The dissipation rate of turbulent kinetic energy

$$\overline{\left(\frac{\nu}{2} \left(\frac{\partial u_i'}{\partial x_j} + \frac{\partial u_j'}{\partial x_i} \right) \left(\frac{\partial u_i'}{\partial x_j} + \frac{\partial u_j'}{\partial x_i} \right) \right)}$$

cannot be obtained directly with the PIV measurements under the present experimental conditions. As previously mentioned, spatial resolution of the interrogation area is not fine enough and could filter the Kolmogorov scale of turbulence (Michelet, 1998). Assuming that the diffusion term of turbulent pressure is negligible $[(1/\rho)(\partial \overline{p' u_j'}/\partial x_i)]$, the dissipation rate of turbulent kinetic energy can be estimated from Eq. 21. In this work, the dimensionless form is used to present data. Transfer terms, transport, diffusion, and dissipation are normalized with $N^3 D^2$.

Kinetic energy transfers between mean, organized, and turbulent motion

The three kinetic energy transfer terms between the three motions have been expressed in Eqs. 22 to 24. Even though their expressions are different, each term is a product of:

• A gradient of velocity $\partial u_i/\partial x_j$ of the mean or organized motion;

• A stress term $\overline{u_i u_j}$ of organized or turbulent motion.

Moreover, each global transfer term is made up of nine components

$$\sum_{i=1}^{3} \sum_{j=1}^{3} \overline{u_i u_j} \frac{\partial u_i}{\partial x_j} \tag{26}$$

The objective is to quantify these terms of transfer between the three motions in a region close to the impeller in order to understand their origin. The calculation of the gradients $\partial/\partial x_j$ is based on a second-order discretization scheme. This technique is performed in each measurement plane at a spatial resolution of 1.25 mm.

Kinetic Energy Transfers Between Mean and Turbulent Motion (Tmt). The transfer of kinetic energy from the mean flow to the turbulence is commonly known as a production term of turbulence in a classic Reynolds decomposition. Figure 10a shows the distribution of the kinetic energy exchange in a vertical plane.

In the impeller-stream jet, the main characteristic is that the kinetic energy is exchanged from the mean motion to the turbulent one. Two regions of high transfer occur above and below the jet axis. The maximum magnitude is about 14 and is located at a radial position close to $r/R = 1.3$.

Kinetic Energy Transfers Between Mean and Organized Motion (Tmo). Figure 10b shows the distribution of kinetic energy transfer (*Tmo*) between the mean and organized motions in the vertical plane. Its expression is based on the stress of organized flow $\overline{\tilde{u}_i \tilde{u}_j}$ and the gradient of the mean velocity $\partial \overline{U_i}/\partial x_j$. This kinetic energy exchange is clearly positive in the impeller jet. Consequently, kinetic energy is transferred from the mean motion to the organized one.

Near the impeller tip ($r/R = 1.07$), the *Tmo* transfer has a high value, close to 14; futher from the blades ($r/R > 1.4$), the magnitude of this transfer is smaller and does not exceed 1.5. This characteristic can be easily understood: the stresses of organized motion and the organized kinetic energy are significant in the impeller vicinity and decrease as radial distance increases. It can be assumed that the majority of the energy exchange takes place in the impeller region, due to high values of organized stresses $\overline{\tilde{u}_i \tilde{u}_j}$. In fact, the trailing vortices are much more coherent near the blade, with large organized velocity components ($\tilde{u}_i$).

Kinetic Energy Transfers Between Organized and Turbulent Motion ($\overline{Tot}$). The expression of kinetic energy transfer between organized and turbulent motions is basically different from previous transfers. The $\overline{Tot}$ term involves:

• r_{ij}, the difference between the phase $\langle u_i' u_j' \rangle$ and time average $\overline{u_i' u_j'}$ of the turbulent Reynolds stress;

• $\partial \tilde{u}_i/\partial x_j$, the gradient of the organized velocity (trailing vortices).

The product of these two components (expressed by *Tot*) is then time averaged to obtain the global transfer term $\overline{Tot}$.

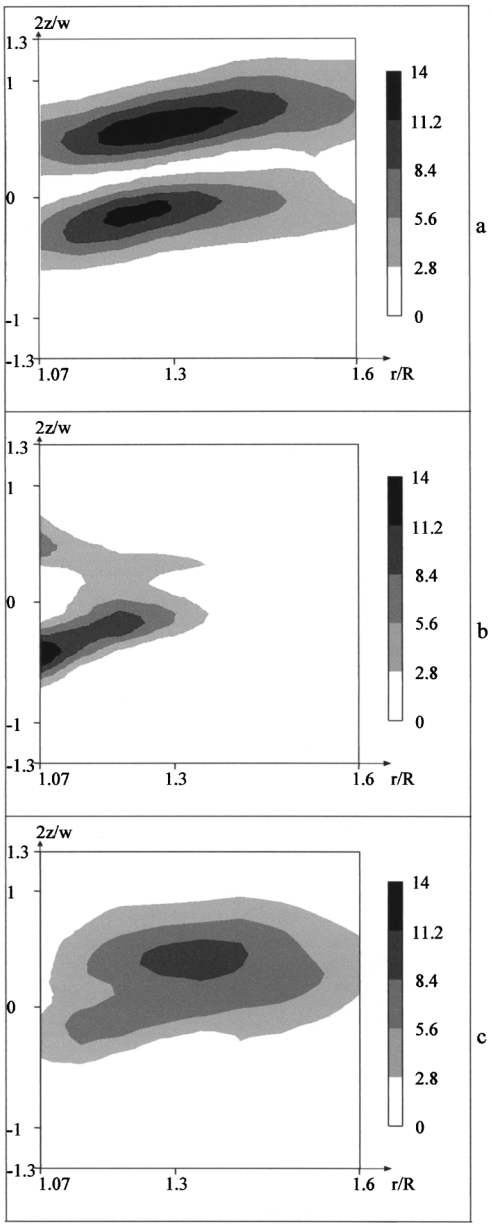

Figure 10. Distribution of the kinetic energy transfers normalized with N^3D^2 in the vertical plane.

(a) Transfer between mean and turbulent motions (***TmT***); (b) transfer between mean and organized motions (***Tmo***); (c) transfer between organized and turbulent motions ($\overline{Tot}$).

Figure 10c gives the distribution of $\overline{Tot}$ in the vertical plane. In the impeller jet, its value is positive with a magnitude close to *Tmt*. A large amount of kinetic energy is transfered from the organized motion to the turbulent one. This quantification can easily explain the increase in turbulent kinetic energy and the decrease in organized kinetic energy in the jet of a Rushton turbine; the kinetic energy of organized motion is then a "source" of turbulence.

The transfer between organized and turbulent flow should be considered without time averaging (*Tot*) in order to be related to the organized structure (trailing vortex). The term *Tot* is plotted in a vertical plane for two angular positions of the blade relative to the measurement plane: Figures 11a and 11b correspond, respectively, to angular positions of 25° and 35° behind the blade. The velocity field of the organized flow enables the location of the trailing vortices to be visualized (Figures 11c and 11d). The transfer of kinetic energy between organized and turbulent flows is located in a region close to the trailing vortices. Indeed, the magnitude of the gradient $\partial \tilde{u}_i/\partial x_j$ is high in a vortex zone and the Reynolds stresses (and r_{ij}) are spatially correlated to the trailing vortices (Lee and Yianneskis, 1998; Sharp and Adrian, 2001; Escudié, 2001). The maximum local value of *Tot* reaches 40; it is four times the value of the time-averaged transfer ($\overline{Tot}$). The locations of trailing vortices are the main regions of the kinetic energy transfer. As a consequence, if the local dissipation rate of turbulent kinetic energy is examined inside the trailing vortices, it could be higher than the dissipation rate usually calculated after time averaging.

Now that the transfers of kinetic energy have been quantified, the balance equation of the kinetic energy of mean flow, organized structure, and turbulence can be analyzed in detail.

Kinetic energy balances

Reynolds and Hussain (1972) derived the kinetic energy balance equations for the three types of the kinetic energy. The goal of this study was to estimate each term of these equations.

Kinetic Energy Balance of Mean Motion. The kinetic energy balance of the mean flow is presented in the Eq. 19 and can be simplified as follows

$$\text{Dissipation} = -\text{Diffusion-transfer } Tmt - \text{transfer } Tmo - \text{transport} \quad (27)$$

The experimental data bank enables all the terms to be calculated, except the diffusion induced by the pressure

$$\left(\frac{1}{\rho}\sum_i \frac{\partial \overline{P}\,\overline{U_i}}{\partial x_i}\right)$$

Since it is the only term that cannot be measured, it will be deduced from the balance equation.

Vertical profiles of the five terms presented in the Eq. 19 are plotted in Figure 12 close to the impeller tip ($r/R = 1.07$) and at $r/R = 1.6$. The viscous dissipation of the kinetic energy of the mean flow is calculated directly from the mean velocity gradient: this term is negligible. The transport of mean kinetic energy by the mean flow is the main term. Its sign is negative with a maximum value close to -60 at $r/R = 1.07$; the kinetic energy carried into this zone is larger than the kinetic energy carried out, since the mean motion transfers kinetic energy both to organized and turbulent flows. The kinetic energy balance of mean motion can be simplified as follows

$$0 \approx -\text{Diffusion-transfer } Tmt - \text{transfer } Tmo - \text{transport} \quad (27a)$$

Kinetic Energy Balance of Organized Motion. The kinetic energy balance equation of organized motion (Eq. 20) can be simplified as follows

$$\text{Dissipation} = -\text{diffusion} + \text{transfer } \textit{Tmo}\text{-transfer } \overline{Tot} - \text{transport} \quad (28)$$

The two kinds of kinetic energy transfer are separated because of their opposite signs in the equation. The diffusion induced by the organized pressure stresses

$$\left(\frac{1}{\rho}\sum_j \frac{\partial}{\partial x_j}\overline{\tilde{u}_j\tilde{p}}\right)$$

is the only term of Eq. 31 that cannot be measured; it will be estimated after balance. Figure 13 plots vertical profiles of the five terms presented in Eq. 28 for $r/R = 1.07$ and for $r/R = 1.6$. The viscous dissipation of organized flow is estimated after experiments and is negligible; its order of magnitude is the same as that of the dissipation of mean flow. Near the impeller tip, the other terms reach significant values. However, at the radial position $r/R = 1.6$, Figure 13b shows an equilibrium between the transport of kinetic energy of organized motion and the transfer of kinetic energy from the organized flow to a turbulent one: the organized motion is a "source" of turbulence

$$\text{Transfer } \overline{Tot} + \text{transport} \approx 0 \quad (28a)$$

Kinetic Energy Balance of Turbulent Motion. One of the objectives of the article is to quantify the dissipation rate of

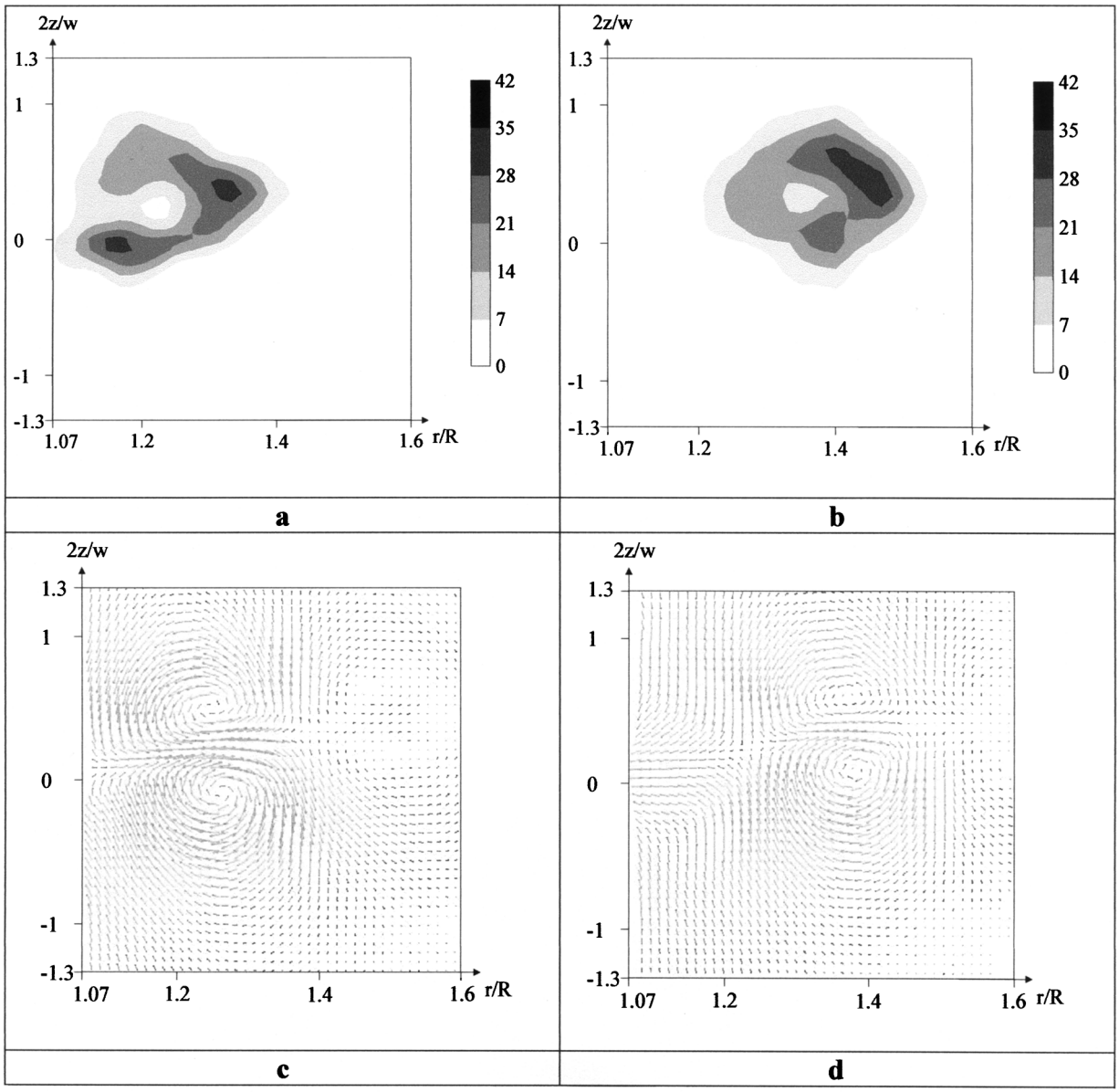

Figure 11. Comparison between the *Tot* transfer level and the trailing vortices position at two angular positions.
(a) Normalized *Tot* (25°); (b) normalized *Tot* (35°); (c) velocity field of organized flow (25°); (d) velocity field of organized flow (35°).

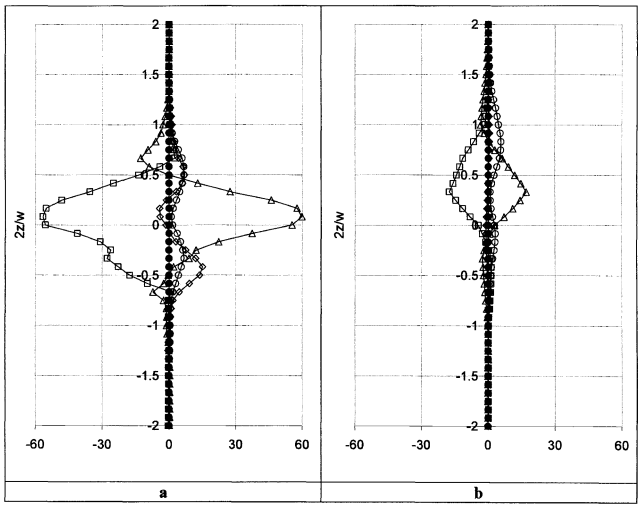

Figure 12. Terms of the kinetic energy balance of mean motion normalized with N^3D^2.

−○− Transfer *Tmt*; −◇− transfer *Tmo*; −□− transport; −△− diffusion; −●− dissipation. (a) Vertical profile at $r/R = 1.07$; (b) vertical profile at $r/R = 1.6$.

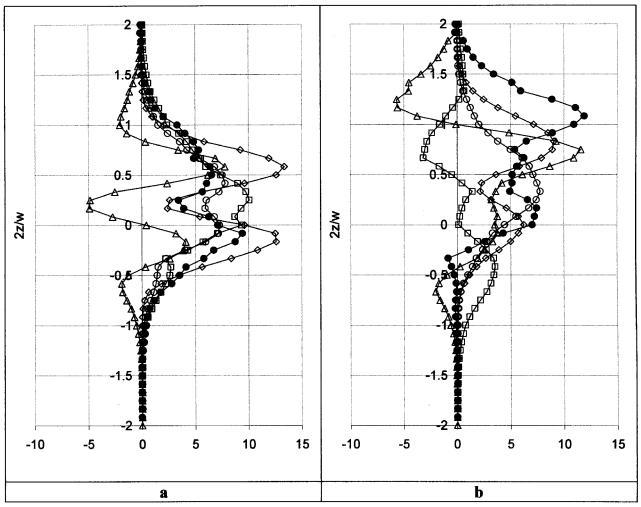

Figure 14. Terms of the kinetic energy balance of turbulent motion normalized with N^3D^2.

−◇− Transfer *TmT*; −○− transfer $\overline{Tot}$; −□− transport; −△− diffusion; −●− dissipation. (a) Vertical profile at $r/R = 1.2$; (b) vertical profile at $r/R = 1.47$.

turbulent kinetic energy. Most of the terms that compose the kinetic energy balance of turbulent motion (Eq. 21)—transport, diffusion, dissipation, and transfer—can be evaluated. The pressure velocity correlation term cannot be calculated from PIV data. If we considered the transport equation of each one of the diagonal components of the Reynolds stress tensor, the pressure velocity correlation would be very important, since it controls the redistribution of TKE; since we consider the balance of TKE, we can refer to results from direct numerical simulation in the pipe flow (Eggels et al., 1994). The authors mention that in the budget of TKE, the pressure−velocity gradient term consists only in the pressure-diffusion term and is of minor importance. The diffusion term generated by turbulent pressure stresses then will be assumed to be negligible. The viscous dissipation of turbulent kinetic energy then can be estimated as follows

$$\text{Dissipation} = -\text{diffusion} + \text{transfer } Tmt + \text{transfer } \overline{Tot} - \text{transport}. \quad (29)$$

Figures 14a and 14b presents a vertical profile of the five terms of Eq. 29, at the radial position $r/R = 1.2$ and $r/R = 1.47$. The transport of turbulent kinetic energy by the mean flow is significant in the impeller jet. From the impeller tip to the radial position $r/R = 1.5$, this term is positive with a value close to 10 near the jet axis; the mean flow carries the turbulent kinetic energy out of this region. Escudié (2001) showed that the transport in the radial direction $(\overline{U_1}(\partial/\partial x_1)/k)$ is the main term. Indeed, there is a radial mean velocity in the jet, and the turbulent kinetic energy increases strongly up to the radial position $r/R \approx 1.4$. The transfer term results from the exchange of kinetic energy from mean to organized motions. It can be considered as a "source term" of turbulent kinetic energy.

Figure 15 shows the spatial distribution of the viscous dissipation rate, ϵ, of the turbulent kinetic energy estimated in the vertical plane. The values of ϵ are higher inside the jet of the impeller than outside. Their magnitudes increase up to a radial position $r/R = 1.4$ and then decrease. Assuming that the baffles located at the wall do not affect the hydrodynamic near the impeller zone, the power dissipated in the fluid volume (P_ν) can be calculated as follows

$$P_\nu = \rho \int_H^{r+\Delta r} \int_r 2\pi r \epsilon \, dr dh \quad (30)$$

Thus, we estimate that 15% of the energy generated by the Rushton turbine is dissipated in the volume of measurement ($1.07 \le r/R \le 1.6$, 120 mm $\le X_3 \le$ 180 mm).

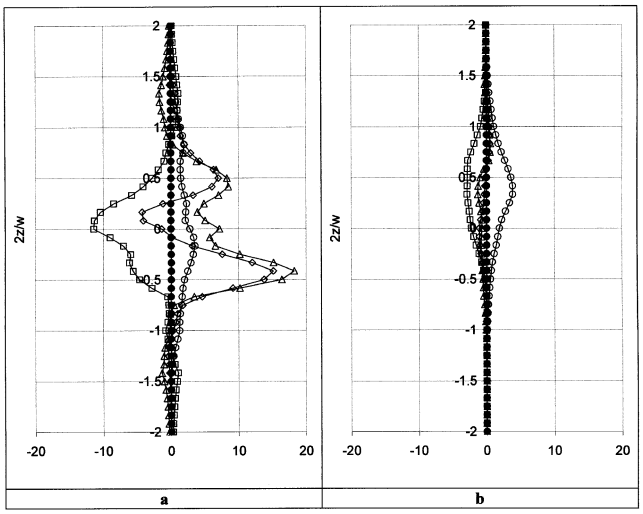

Figure 13. Terms of the kinetic energy balance of organized motion normalized with N^3D^2.

−◇− Transfer *Tmo*; −○− transfer $\overline{Tot}$; −□− transport; −△− diffusion; −●− dissipation. (a) Vertical profile at $r/R = 1.07$; (b) vertical profile at $r/R = 1.6$.

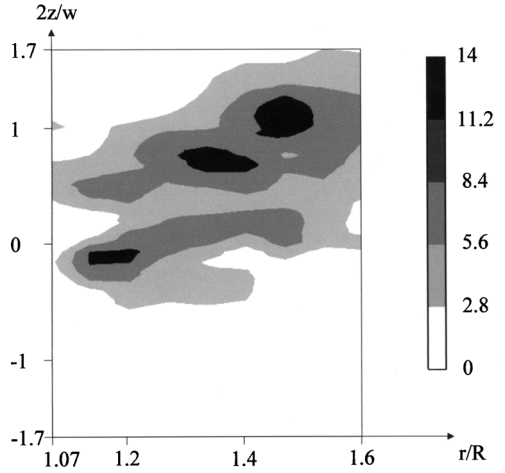

Figure 15. Viscous dissipation ϵ of turbulent kinetic energy normalized with N^3D^2 in the vertical plane.

Turbulent Scales

Three kinds of turbulent length-scales can be estimated. The previous estimation of the dissipation rate of turbulent kinetic energy will be used. Both the Kolmogrov scale (η) and the Taylor microscale (λ) are calculated with Eqs. 1 and 2, respectively. The macrolength scale (Λ) can be estimated directly from cross-correlation of turbulent velocity fields.

Kolmogrov scale (η) and Taylor microscale (λ)

The Kolmogrov scale (η) and Taylor microscale (λ) are plotted in the Figures 16a and 16b, respectively, in the vertical plane of the measurement.

The Kolmogrov scale ranges from 20 μm to 40 μm in the jet; it increases to 100 μm outside the jet. The Taylor microscale lies between 500 μm and 1 mm in the jet, and it reaches a maximal value of 3 mm outside the jet. This order of magnitude is coherent with the spatial resolution of the PIV technique.

Macrolength scale ($\overline{\Lambda}$)

Since the PIV gives instantaneous velocity fields in a plane, it is possible to determine spatial cross-correlations of the turbulent velocities. Spatial-velocity correlation functions can be defined as follows

$$R_{ij}(M,dX_k) = \frac{\overline{u_i'(M)u_j'(M+dX_k)}}{\sqrt{\overline{u_i'^2}(M)}\sqrt{\overline{u_j'^2}(M+dX_k)}} \qquad (31)$$

The indices i and j are related to the velocity components, the component i taken at the reference position, the component j taken at a different location in the direction k. From these functions, a large number of integral turbulent length scales can be determined in the following form

$$\Lambda_{ijk} = \int_0^{+\infty} R_{ij}(M,dX_k)\,dX_k \qquad (32)$$

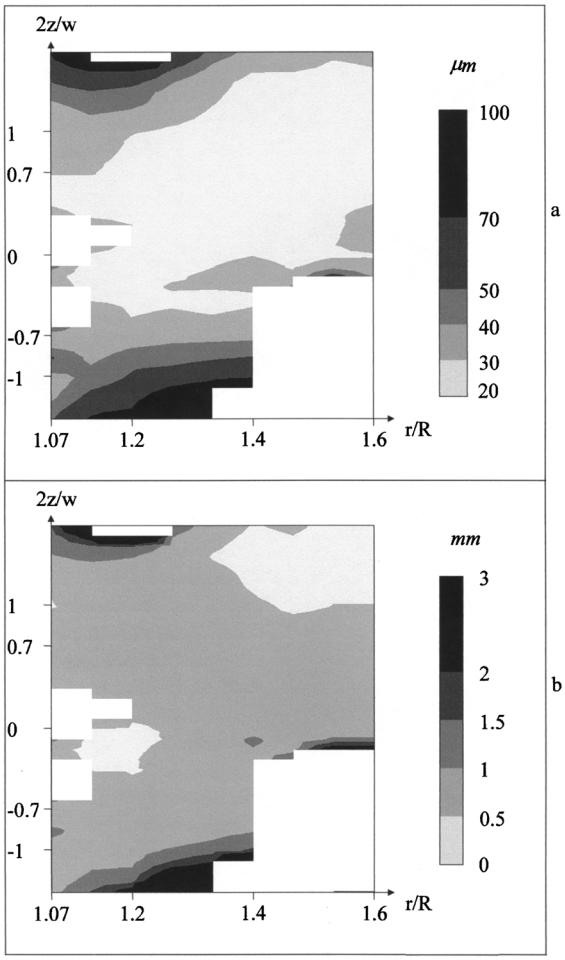

Figure 16. Turbulent scales in the vertical plane of measurement.

(a) Kolmogrov scale (η); (b) Taylor microscale (λ).

The longitudinal integral scale Λ_f corresponds to the characteristic length scale of the energy containing eddies (Hinze, 1959). Since the turbulence is not homogeneous and not isotropic, the integral scales Λ_{111}, Λ_{222}, and Λ_{333} are different. Moreover, near the impeller zone, spatial-velocity correlation functions must be calculated from phase-average data, because the turbulence characteristics depend on the angular position of the blade relative to the measurement plane. Escudié (2001) shows that the integral scales Λ_{iii}^k vary enormously between two successive blades.

At a measurement point, the average integral scale $\overline{\Lambda_{iii}}$ is calculated as follows

$$\overline{\Lambda_{iii}} = \sum_{k=1}^{N_p} \frac{\Lambda_{iii}^k}{Np} \qquad (33)$$

The averaged macrolength scale $\overline{\Lambda}$ is defined by (Hinze, 1959; Wu and Patterson, 1989)

$$\overline{\Lambda} = \sqrt{(\Lambda_{111})^2 + (\Lambda_{222})^2 + (\Lambda_{333})^2} \qquad (34)$$

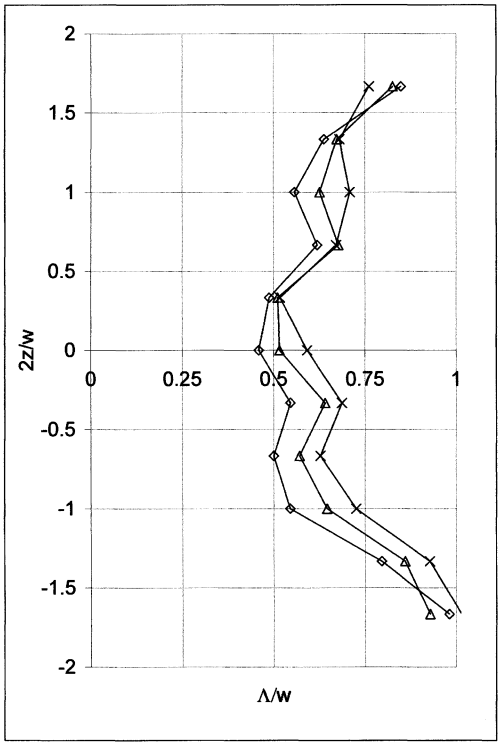

Figure 17. Vertical profiles of averaged macrolength scale $\overline{\Lambda}$ for three radial positions.

--◇-- $r/R = 1.07$; -- △ -- $r/R = 1.2$; --×-- $r/R = 1.33$.

Figure 17 presents vertical profiles of $\overline{\Lambda}$ at three radial positions in the impeller jet. Near the impeller tip ($r/R = 1.07$), in the projection of the blade height, the macrolength scale, $\overline{\Lambda}$, ranges between $0.45w$ and $0.55w$. This length is the characteristic value of the radial jet that generates the macroturbulent eddies. When the radial position increases, the magnitude of $\overline{\Lambda}$ increases to $0.7w$ at $r/R = 1.33$. For example, between the positions $r/R = 1.07$ and 1.2 (40 mm), the turbulent macrostructures vary from $0.05w$ (1.5 mm) to $0.15w$ (5 mm). Also, $\overline{\Lambda}$ increases linearly above and below the stream jet region. These results are in agreement with previous works: Costes and Couderc (1988), $\overline{\Lambda} = 0.45w$; Mahouast et al. (1989), $0.48 < \overline{\Lambda} < 1.32$; Michelet (1998), $0.6 < \overline{\Lambda} < 1.2$. However, in the present work, the macro length-scale, $\overline{\Lambda}$, is calculated directly from turbulent velocity fields, without any assumptions. This technique takes into account the turbulence anisotropy and the fact that the turbulence characteristic depends on the blade position in the vicinity of the impeller.

As previously mentioned, the usual way to estimate the dissipation rate of turbulent kinetic energy is based on dimensional analysis

$$\epsilon = A\frac{k^{3/2}}{\Lambda} \tag{35}$$

with $A = 1$. Since the dissipation rate of TKE has been estimated, the validity of this correlation can be tested. Starting from the phase-averaged data in the k-plane relative to the blade position, it is possible to calculate the phase-averaged dissipation $\langle \epsilon \rangle^k$ from the macrolength scale (Λ^k) and the turbulent kinetic energy $\langle k \rangle^k$, as follows

$$\langle \epsilon \rangle^k = \frac{\langle k \rangle^{k3/2}}{\langle \Lambda \rangle^k} \tag{36}$$

Thus, the averaged dissipation ϵ was estimated by

$$\epsilon = \sum_{k=1}^{Np} \frac{\langle \epsilon \rangle^k}{Np} \tag{37}$$

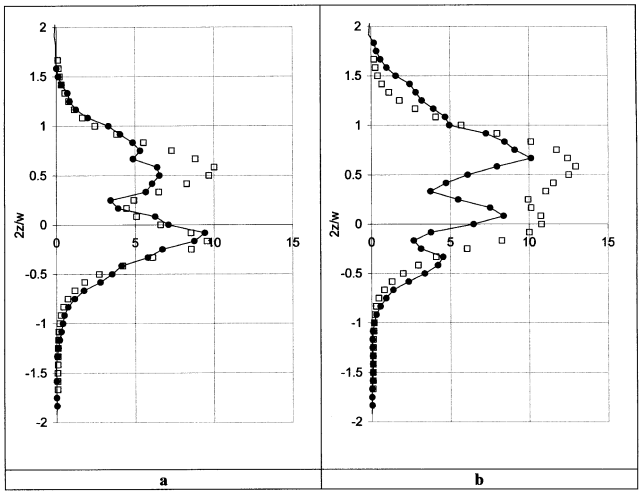

Figure 18. Vertical profiles of ϵ normalized with N^3D^2 for two radial positions.

Estimated from ● turbulent kinetic energy balance, □ dimensional analysis. (a) $r/R = 1.2$; (b) $r/R = 1.33$.

The vertical profiles of ϵ are plotted in Figures 18a and 18b for the radial positions ($r/R = 1.2$ and 1.33). In the jet region, the correlation (Eq. 35) relating ϵ to the macrolength scale overestimates the dissipation rate. Indeed, the dimensional analysis assumes that the turbulence is fully developed; in this case, an equilibrium occurs between the dissipation rate and the production (transfer between mean and turbulent motion). This condition is not verified in the case of the radial jet of the Rushton turbine. The analysis of kinetic energy balances of turbulent motion has shown that two additional terms are significant in this region: the transport and the kinetic energy transfer from organized to turbulent motion.

Outside the jet, there is good agreement between the two estimations of the dissipation rate of TKE. Indeed, in these regions, the transport term and the transfer from organized to turbulent motion are lower.

Summary and Conclusion

In the first part of this article, the principles of the PIV technique were recalled. The experimental setup was presented. The apparatus used in this study consists of a standard cylindrical tank equipped with a Rushton turbine. Ex-

periments were carried out at a single value of impeller rotational speed, $N = 150$ rpm. The accuracy of the data acquisition and processing was assessed. A data bank has been developed. It consists of the three components of the velocity vector and the six components of the stress tensors (turbulent and organized motions) that are available in a vertical plane between r/R of 1.06 and 1.6, and between X_3 of 130 mm and 170 mm. Resolved angle measurements were made. The Rushton turbine is a six-bladed impeller with equally spaced blades. As a consequence, given 1-deg angle-resolved measurements, it was necessary to perform 60 planes to reconstruct the flow between two successive blades.

The mean velocity field and the Reynolds stress components were analyzed and validated. The turbulent kinetic energy increases by a factor of 2 between the impeller tip and radial position, $r/R = 1.4$; further away, the turbulent kinetic energy decays rapidly. This turbulent kinetic energy increase is significant and is related to the decrease in periodic kinetic energy in the same region. As a consequence, the kinetic energy transfer between periodic and turbulent components was analyzed.

In the impeller stream jet, the main characteristic is that the kinetic energy is exchanged from the mean motion to the turbulent and organized ones. A significant amount of kinetic energy is transferred from the organized motion to the turbulent one. The transfer of kinetic energy between organized and turbulent flows is located in a region close to the trailing vortices. Once the transfer of kinetic energy had been quantified, the balance equation of kinetic energy of the mean flow, organized structure, and turbulence was analyzed in detail.

Concerning the kinetic energy of the mean flow, the viscous dissipation was calculated directly from the mean velocity gradient and found to be negligible. The transport of mean kinetic energy by the mean flow is the main term. Its sign is negative, and the kinetic energy carried into this zone is larger than the kinetic energy carried out, since the mean motion transfers kinetic energy both to organized and turbulent flows.

Concerning the organized flow, the viscous dissipation was estimated from experiments and was negligible. Near the impeller tip, the other terms of the kinetic energy balance reach significant values. However, at the larger radial position, an equilibrium between the transport and the transfer of kinetic energy from organized flow to a turbulent one was observed.

Concerning the turbulence, the diffusion term generated by turbulent pressure stresses cannot be calculated from the PIV data and has been assumed to be negligible. The viscous dissipation of TKE was then estimated from the TKE balance equation. The transport of TKE by the mean flow is significant in the impeller jet. This term is positive, and the mean flow carries the TKE outside this region. Different transfers result from the exchange of kinetic energy from both the mean and organized motions to turbulence. They can be considered as "source terms" of TKE. It was estimated that 15% of the energy generated by the Rushton turbine is dissipated in the volume of measurement.

Three kinds of turbulent length-scales were then estimated: the Kolmogrov scale (η), the Taylor microscale (λ) and the macrolength scale (Λ). The Kolmogrov scale ranges between 20 and 40 μm in the stream jet; it increases to 100 μm outside the jet. The Taylor microscale is between 500 μm and 1 mm in the jet, and it reaches a maximal value of 3 mm outside the jet. This order of magnitude is coherent with the spatial resolution of the PIV technique. Near the impeller tip, the macrolength scale $\overline{\Lambda}$ ranges between $0.45w$ and $0.55w$. This length is the characteristic value of the radial jet that generates the macroturbulent eddies. When the radial distance increases, the magnitude of $\overline{\Lambda}$ increases to $0.7w$ at $r/R = 1.33$. Moreover, $\overline{\Lambda}$ increases linearly above and below the stream jet region.

Acknowledgment

The financial support provided by Ministère de l'Education Nationale et de la Recherche and Région Midi-Pyrénées is gratefully acknowledged.

Notation

B = baffle width, m
C = impeller clearance, m
D = impeller diameter, m
d_p = seeding particle diameter, m
H = liquid height in the tank, m
k = turbulent kinetic energy, m^2/s^2
$\tilde{k}$ = organized kinetic energy, m^2/s^2
k_{total} = total fluctuating kinetic energy, m^2/s^2
N = rotational speed, rev/s
n_e = acquisition number per measurement plane
n_p = plane number between two successive blades
N_P = power number
N_{Q_p} = pumping number
P = power input, W
Q_p = pumping flow rate, m^3/s
Re = Reynolds number
T = tank diameter, m
t_b = blade thickness, m
t_d = disk thickness, m
t_E = temporal macroscale, s
Tmo = kinetic energy transfer between mean and organized motion, m^2/s^3
Tmt = kinetic energy transfer between mean and turbulent motion, m^2/s^3
$\overline{Tot}$ = averaged kinetic energy transfer between organized and turbulent motion, m^2/s^3
U,u = velocity component, m/s
U_{tip} = tip velocity, m/s
$\langle U_i^k(M,t)\rangle$ = phase averaged velocity in the k plane, m/s
$\tilde{u}_i^k(M,t)$ = organized periodic velocity in the k plane, m/s
w = impeller width, m
X_3 = axial distance, m

Greek letters

ϑ = tank volume, m^3
ϵ = dissipation rate of turbulent kinetic energy, m^2/s^3
η = Kolmogrov scale, m
λ = Taylor microscale, m
Λ = macrolength scale, m
ν = kinematic viscosity, m^2/s
ρ = fluid density, kg/m^3

Literature Cited

Bouillard, J., B. Alban, P. Jacques, and C. Xuereb, "Liquid Flow Velocity Measurements in a Stirred Tank by Ultra-Sound Doppler Velocimetry," *Chem. Eng. Sci.*, **56**, 747 (2001).

Bugay, S., "Analyse Locale des Échelles Caractéristiques du Mélange: Application de la Technique P.I.V. aux Cuves Agitées," Thèse de Doctorat de l'Institut National des Sciences Appliquées, Toulouse, France (1998).

Bugay, S., R. Escudié, and A. Liné, "Experimental Analysis of Mean Flow and Turbulence Structure in Agitated Tank Based on PIV Technique with Axial Impeller," *AIChE J.*, **48**(3), 463 (2002).

Costes, J., and J. P. Couderc, "Influence of the Size of the Units: I. Mean Flow and Turbulence," *Chem. Eng. Sci.*, **43**, 2751 (1988).
Cutter, L. A., "Flow and Turbulence in a Stirred Tank," *AIChE J.*, **12**, 35 (1966).
Derksen, J. J., M. S. Doelman, and H. E. A. Van Den Akker, "Three-Dimensional LDA Measurements in the Impeller Region of a Turbulently Stirred Tank," *Exp. Fluids*, **27**, 522 (1999).
Eggels, J. G., F. Unger, J. Westerweel, R. J. Adrian, R. Friedrich, and F. T. M. Nieuwstadt, "Fully Developed Turbulent Pipe Flow: A Comparison Between Direct Numerical Simulation and Experiment," *J. Fluid Mech.*, **268**, 175 (1994).
Escudié, R., "Structure Locale de l'Hydrodynamique Générée par une Turbine de Rushton," Thèse de Doctorat de l'Institut National des Sciences Appliquées, Toulouse, France (2001).
Hill, D. F., K. V. Sharp, and R. J. Adrian, "Stereoscopic Particule Image Velocimetry Measurements of the Flow Around a Rushton Turbine," *Exp. Fluids*, **29**, 478 (2000).
Keane, R. D., and R. J. Adrian, "Theory of Cross-Correlation Analysis of P.I.V. Images," *Appl. Sci. Res.*, **49**, 191 (1992).
Kresta, S. M., "Characterisation Measurement and Prediction of the Turbulent Flow in Stirred Tanks," PhD Thesis, McMaster Univ., Hamilton, Ont., Canada (1991).
Kresta, S. M., and P. E. Wood, "Prediction of the Three-Dimensional Turbulent Flow in Stirred Tanks," *AIChE J.*, **37**(3), 448 (1991).
Lee, K. C., and M. Yianneskis, "Turbulence Properties of the Impeller Stream of a Rushton Turbine," *AIChE J.*, **44**, 13 (1998).
Mahouast, M., G. Cognet, and R. David, "Two-Component LDV Measurements in a Stirred Tank," *AIChE J.*, **35**, 1770 (1989).
Mavros, P., "Flow Visualisation in Stirred Vessels—A Review of Experimental Techniques," *Trans. Inst. Chem. Eng.*, **79**, 113 (2001).
Michelet, S., "Turbulence et Dissipation au Sein d'un Réacteur Agité par une Turbine Rushton—Vélocimétrie Laser Doppler à Deux Volumes de Mesure," Thèse de Doctorat de l'Institut National Polytechnique de Lorraine, Nancy, France (1998).
Mujumbar, A. S., B. Huang, D. Wolf, M. E. Weber, and W. S. M. Douglas, "Turbulence Parameters in a Stirred Tank," *Can. J. Chem. Eng.*, **48**, 475 (1970).
Okamota, Y., M. Nishikawa, and K. Hashimoto, "Energy Dissipation Rate Distribution in Mixing Vessels and Its Effects on Liquid-Liquid Dispersions and Solid-Liquid Mass Transfer," *Int. Chem. Eng.*, **21**, 88 (1981).
Ranade, V. R., and J. B. Joshi, "Flow Generated by a Disc Turbine: Part I: Experimental," *Trans. Inst. Chem. Eng.*, **68**, 63 (1990).
Ranade, V. R., M. Perrard, N. Le Sauze, C. Xuereb, and J. Bertrand, "Trailing Vortices of Rushton Turbine: PIV Measurements and CFD Simulations with Snapshot Approach," *Trans. Inst. Chem. Eng.*, **79** (Part A), 3 (2001).
Reynolds, W. C., and A. K. M. F. Hussain, "The Mechanics of an Organized Wave in Turbulent Shear Flow. Part 3. Theoretical Models and Comparisons with Experiments," *J. Fluid Mech.*, **54** (Part 2), 263 (1972).
Roustan, M., J.-C. Pharamond, and A. Liné, *Techniques de l'Ingénieur, traité Génie des procédés. Agitation, Mélanges*, Techniques de l'Ingénieur, Paris (1999).
Rutherford, K., M. S. Mahmoudi, K. C. Lee, and M. Yianneskis, "The Influence of Rushton Impeller Blade and Disk Thickness on the Mixing Characteristics of the Stirred Vessels," *Trans. Inst. Chem. Eng.*, **74**, 369 (1996).
Saarentine, P., and M. Piirto, "Turbulent Kinetic Energy Dissipation Rate from PIV Velocity Vectors Fields," *Exp. Fluids*, 300 (2000).
Schaffer, M., J. Yu, B. Geneger, and F. Durst, "Turbulence Generation by Different Types of Impellers," *Proc. 10th European Conf. on Mixing*, Delft, The Netherlands, p. 9 (2000).
Schaffer, M., M. Hofken, and F. Durst, "Detailed LDV Measurements for the Visualisation of the Flow Field Within a Stirred-Tank Reactor Equipped with a Rushton Turbine," *Trans. Inst. Chem. Eng.*, **75**, 729 (1997).
Sharp, K. V., and R. J. Adrian, "PIV Study of Small-Scale Flow Structure Around a Rushton Turbine," *AIChE J.*, **47**, 766 (2001).
Sheng, J., H. Meng, and R. O. Fox, "A Large Eddy PIV Method for Turbulence Dissipation Rate Estimation," *Chem. Eng. Sci.*, **55**, 4423 (2000).
Stoots, C., and R. V. Calabrese, "Mean Velocity Field Relative to a Rushton Turbine Blade," *AIChE J.*, **41**, 1 (1995).
Van der Molen, K., and H. R. E. Van Maanen, "Laser-Doppler Measurements of the Turbulent Flow in Stirred Vessels to Establish Scaling Rules," *Chem. Eng. Sci.*, **33**, 1161 (1978)
Wu, H., and G. K. Patterson, "Laser-Doppler Measurements of Turbulent Flow Parameters in a Stirred Mixer," *Chem. Eng. Sci.*, **44**, 2207 (1989).
Yianneskis, M., "Trailing Vortex, Mean Flow and Turbulence Modification Through Impeller Blade Design in a Stirred Reactor," *Proc. Euro. Conf. on Mixing*, Delft, The Netherlands, p. 1 (2000).
Yianneskis, M., Z. Popiolek, and J. H. Whitelaw, "An Experimental Study of the Steady and Unsteady Flow Characteristics of Stirred Reactors," *J. Fluid Mech.*, **175**, 537 (1987).
Yianneskis, M., and J. H. Whitelaw, "On the Structure of the Trailing Vortices Around Rushton Turbine Blades," *Trans. Inst. Chem. Eng.*, **71**, 543 (1993).
Zhou, G., and S. M. Kresta, "Distribution of Energy Between Convective and Turbulent Flow for Three Frequently Used Impellers," *Trans. Inst. Chem. Eng.*, **74**, 379 (1996a).
Zhou, G., and S. M. Kresta, "Impact of the Geometry on the Maximum Turbulence Energy Dissipation Rate for Impellers," *AIChE J.*, **42**, 2476 (1996b).

Manuscript received Mar. 29, 2002, and revision received Sept. 12, 2002.